NASA TECHNICAL NOTE

NASA TN D-6706

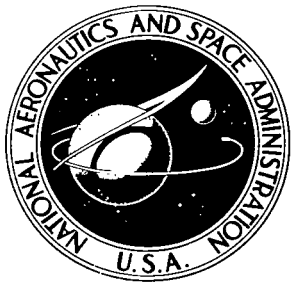

EFFECTS OF RADIAL AND CIRCUMFERENTIAL INLET VELOCITY PROFILE DISTORTIONS ON PERFORMANCE OF A SHORT-LENGTH DOUBLE-ANNULAR RAM-INDUCTION COMBUSTOR

by Donald F. Schultz and Porter J. Perkins

Lewis Research Center
Cleveland, Ohio 44135

NATIONAL AERONAUTICS AND SPACE ADMINISTRATION • WASHINGTON, D. C. • MARCH 1972

1. Report No.	2. Government Accession No.	3. Recipient's Catalog No.
NASA TN D-6706		

4. Title and Subtitle: EFFECTS OF RADIAL AND CIRCUMFERENTIAL INLET VELOCITY PROFILE DISTORTIONS ON PERFORMANCE OF A SHORT-LENGTH DOUBLE-ANNULAR RAM-INDUCTION COMBUSTOR

5. Report Date: March 1972

6. Performing Organization Code:

7. Author(s): Donald F. Schultz and Porter J. Perkins

8. Performing Organization Report No.: E-6464

9. Performing Organization Name and Address:
Lewis Research Center
National Aernautics and Space Administration
Cleveland, Ohio 44135

10. Work Unit No.: 764-74

11. Contract or Grant No.:

12. Sponsoring Agency Name and Address:
National Aeronautics and Space Administration
Washington, D.C. 20546

13. Type of Report and Period Covered: Technical Note

14. Sponsoring Agency Code:

15. Supplementary Notes:

16. Abstract

Inlet air velocity profile tests were conducted on a full-scale short-length 102-centimeter-(40-in.-) diameter annular combustor designed for advanced gas turbine engine applications. The inlet profiles studied include radial distortions that were center peaked, and tip peaked, as well as a circumferential distortion which was center peaked for one-third of the circumference and flat for the other two-thirds. An increase in combustor pressure loss was the most significant effect of the radial air velocity distortions. With the circumferential distortion, exit temperature pattern factor doubled when compared to a flat inlet velocity profile.

17. Key Words (Suggested by Author(s))	18. Distribution Statement
Jet engine; Combustors (annular); Combustion; Hydrocarbon combustion; Combustion efficiency; Diffuser radial profile; Diffuser circumferential profile; Pattern factor; Stator factor; Rotor factor	Unclassified - unlimited

19. Security Classif. (of this report)	20. Security Classif. (of this page)	21. No. of Pages	22. Price*
Unclassified	Unclassified	43	$3.00

*For sale by the National Technical Information Service, Springfield, Virginia 22151

CONTENTS

EFFECTS OF RADIAL AND CIRCUMFERENTIAL INLET VELOCITY PROFILE DISTORTIONS ON PERFORMANCE OF A SHORT-LENGTH DOUBLE-ANNULAR RAM-INDUCTION COMBUSTOR

by Donald F. Schultz and Porter J. Perkins

Lewis Research Center

SUMMARY

Inlet air velocity profile tests were conducted on a full-scale short-length 102-centimeter- (40-in.-) diameter annular combustor designed for advanced gas turbine engine applications. The combustor was originally designed for a large turbofan engine operating at flight speeds up to Mach 3.0. The inlet profiles studied include radial distortions that were center peaked and tip peaked. A circumferential distortion which was center peaked for one-third of the circumference and flat for the other two-thirds was also tested.

Combustion efficiency, air distribution, and exit temperature profile were affected little by the different radial airflow profiles. An increase in combustor pressure loss was the most significant effect. However, with the circumferential distortion, combustor exit temperature pattern factor deteriorated. At a simulated takeoff condition with an average combustor temperature rise of 750 K (1350° F) pattern factor increased from 0.245 to 0.530 with the circumferential distortion compared to the flat inlet velocity profile.

INTRODUCTION

Previous tests of this short-length double-annular ram-induction combustor (ref. 1) were conducted with flat airflow profiles entering the combustor. However, jet engine combustors seldom have flat inlet air profiles. They are commonly center or tip peaked and occasionally also circumferentially nonuniform. Circumferentially nonuniform profiles were reported in reference 2 for a research compressor with 120° of circumferential inlet distortion using screens to distort that sector.

Airflow distortions result from the compressor design, engine inlet design, and aircraft attitude. To perform satisfactorily a combustor must be insensitive to the inlet air profile, or the profile must be tailored to the combustor by modifying the engine inlet, compressor, or combustor diffuser.

One of the more outstanding characteristics of the ram-induction combustor is that its exit temperature profile is very insensitive to the radial inlet velocity profile. Previous tests of a single-annular ram-induction combustion (ref. 3) have demonstrated this characteristic. While such combustors have shown the ability to provide a satisfactory exit temperature profile with a radially distorted inlet air profile, the effects of a circumferentially distorted profile are not generally known. A circumferentially distorted profile would be expected to produce a more serious effect of high exit temperatures in the regions of low airflow.

For these tests the airflow was distorted from a flat inlet velocity profile to a center peaked profile, a tip peaked profile, and a circumferential distorted profile. This was done by inserting punched plates a short distance upstream of the diffuser inlet. In all cases, the punched plate extended only part way across the inlet annulus leaving at least the center area fully unobstructed.

The effects of various radially and circumferentially distorted steady-state airflows on the combustor pressure loss, exit temperature profiles, and pattern factors are presented. The investigation was conducted in a full-scale engine component, connected-duct research facility at the Lewis Research Center.

Appendixes A to E give details concerning reported symbols, combustor design, test facility, instrumentation, and calculations, respectively.

AIRFLOW DISTORTION PLATES

To undertake this study, it was necessary to develop a technique of distorting the airflow profile near the outer and inner walls of the diffuser inlet. Punched plate extending perpendicularly from each wall into the constant area section of the diffuser inlet was found to be satisfactory. Figure 1(a) shows the axial location of the distortion plates, while figure 1(b) shows the distortion plate location used with the circumferential airflow profile.

Figure 2 is a photograph of the airflow distortion plates used. The punched plates had 29 percent open area with 0.084-centimeter (0.033-in.) holes, and were 0.061 centimeter (0.024 in.) thick. The support backing plate is 0.318 centimeter (0.125 in.) thick and 1.905 (0.75 in.) wide. The outer diameter plate was 0.968 centimeter (0.381 in.) wide (extension from wall of diffuser) while the inner diameter plate was 1.286 centimeter (0.506 in.) wide. The plates were made in segments. They were installed

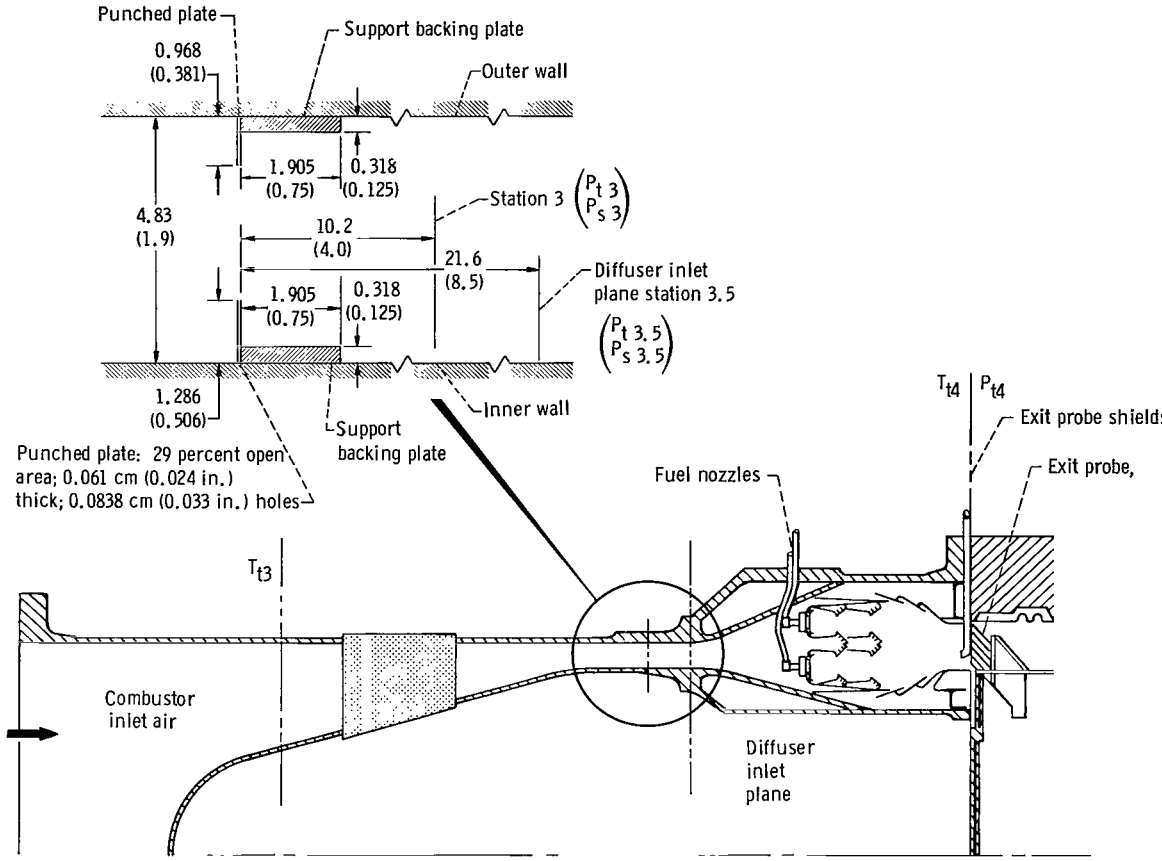

(a) Axial location.

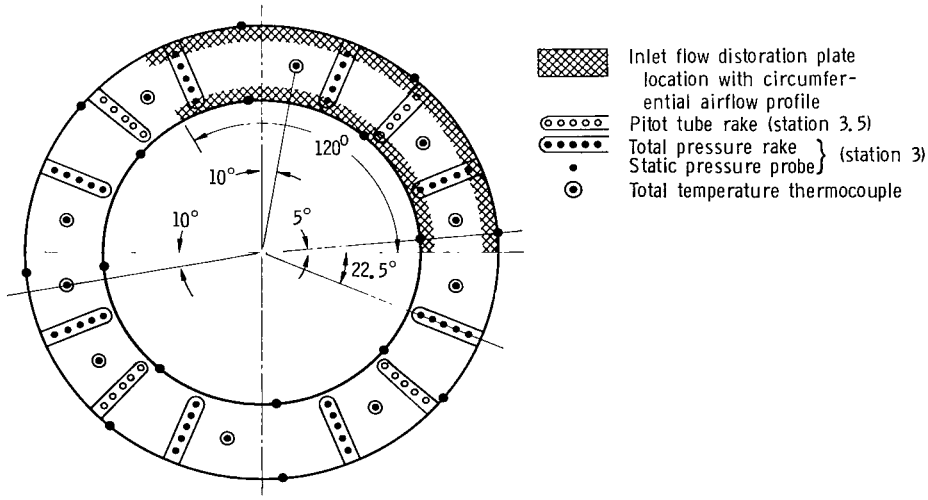

(b) Circumferential location. Diffuser inlet instrumentation covering distortion plate station through station 3.5. View looking downstream

Figure 1. - Location of combustor instrumentation. (All dimensions in cm (in.) unless otherwise indicated.)

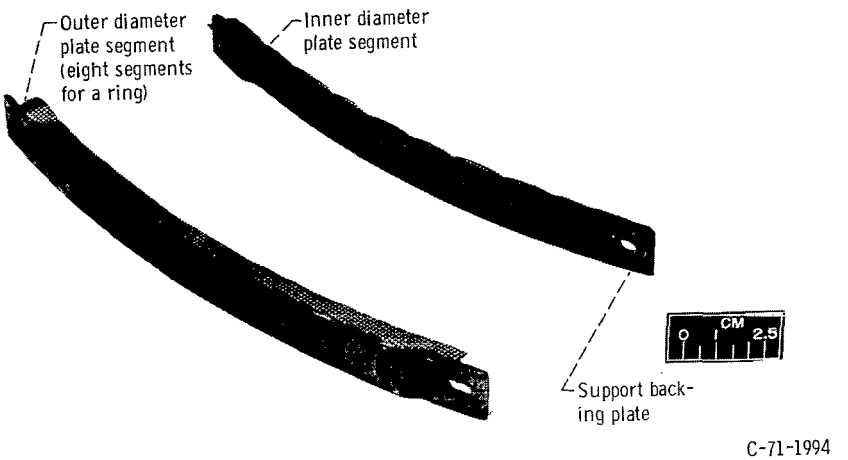

Figure 2. - Inlet airflow distortion plates.

with pins extending from the outer housing to the inner diameter housing and located behind diffuser inlet struts.

For these tests, four inlet velocity profiles were used; namely, flat, center peaked, tip peaked (peaked toward the outer diameter), and circumferentially distorted. For the flat inlet velocity profile no plates were installed. The center peaked profile used plates on both the inner and outer walls of the passage, while the tip peaked inlet velocity profile used only the inside diameter plates. For comparison of results, the circumferentially distorted inlet velocity profile utilized the flat inlet velocity profile for two-thirds of the inlet circumference and the center peaked inlet velocity profile for the remaining one-third.

TEST CONDITIONS

Simulated sea-level takeoff and Mach 2.7 cruise were the two combustor test con-

TABLE I. - SIMULATED OPERATING CONDITIONS

	Takeoff	Mach 2.7 cruise
Inlet air temperature, K (^{o}F)	589 (600)	839 (1050)
Inlet air total pressure, N/m^2 abs (psia)	62 (90)	41 (60)
Reference velocity, m/sec (ft/sec)	30.5 (100)	45.7 (150)
Exit average temperature, K (^{o}F)	1478 (2200)	1478 (2200)
Temperature rise, K (^{o}F)	889 (1600)	639 (1150)

TABLE II. - DATA TABLE

Run	Inlet air conditions									Combustor operating conditions							Combustor performance characteristics						
	Velocity profile	Total pressure		Total temperature		Airflow		Diffuser inlet Mach number	Reference velocity		Fuel air ratio	Average outlet temperature		Inlet fuel temperature		Fuel nozzle differential pressure		Pattern factor	Stator factor	Rotor factor	Combustor average temperature rise		Combustor pressure loss, percent	Composition efficiency, percent
		N/cm^2 abs	psia	K	°F	kg/sec	lb/sec		m/sec	ft/sec		K	°F	K	°F	N/cm^2	psi				K	°F		
157	Flat	62.1	90.1	594	609	50.4	111.0	0.252	32.2	105.6	------	----	----	---	---	-----	-----	-----	-----	------	---	----	5.80	-----
175		62.5	90.6	587	598	49.5	109.1	.249	31.1	102.1	0.0211	1358	1984	289	61	159	230	0.238	0.234	0.0385	770	1387	5.95	104.0
176		62.7	90.9	590	603	49.3	108.6	.243	31.0	101.8	.0255	1497	2235	289	60	229	332	.270	.240	.0618	907	1633	5.91	103.5
177		63.5	92.1	588	599	50.1	110.5	.244	31.1	102.0	.0252	1489	2221	288	59	233	338	.266	.236	.0623	901	1622	5.89	103.7
181		42.6	61.8	841	1054	33.4	73.6	.297	44.1	144.7	.0185	1475	2195	288	59	55	81	.219	.190	.0236	634	1141	8.22	101.7
182		42.7	61.9	840	1052	33.4	73.6	.296	43.9	144.1	.0186	1476	2196	290	62	56	81.5	.213	.204	.0236	636	1144	8.30	101.9
184		42.6	61.8	841	1053	33.3	73.4	.296	44.0	144.2	.0186	1479	2203	290	63	56.5	82	.206	.202	.0239	639	1150	8.24	102.1
185		41.6	60.4	841	1054	34.7	76.5	.319	46.9	153.8	------	----	----	---	---	-----	-----	-----	------	------	---	----	9.22	-----
274	Center peaked	61.8	89.6	589	601	47.3	104.2	.248	30.0	98.4	------	----	----	---	---	-----	-----	-----	------	------	---	----	7.58	-----
275		62.0	89.9	587	596	47.4	104.5	.247	29.8	97.9	.0133	1097	1515	301	82	57	82	.262	.243	.0518	511	919	7.74	105.3
276	Center peaked	62.1	90.1	590	602	47.3	104.3	.247	29.9	98.1	.0166	1217	1730	299	79	90	131	.290	.262	.0486	627	1128	7.80	105.4
277		62.0	89.9	589	600	47.3	104.2	.247	29.9	98.1	.0201	1336	1946	299	79	133	194	.306	.289	.0613	747	1345	7.82	105.7
278		62.0	90.0	587	597	47.2	104.2	.246	29.7	97.6	.0237	1452	2154	300	80	184	268	.320	.292	.0844	865	1558	7.74	105.7
280		43.6	63.3	842	1056	33.9	74.8	.318	43.4	142.5	.0098	1191	1683	312	102	15	22	.252	.244	.0216	348	627	11.63	102.1
282		43.5	63.0	841	1053	34.1	75.2	.320	43.7	143.4	.0132	1309	1897	304	87	29	43	.259	.253	.0350	469	843	11.77	103.3
283	Center peaked	43.9	63.6	840	1052	34.0	75.0	.316	43.2	141.7	.0164	1413	2084	303	85	46	67	.242	.238	.0386	574	1032	11.52	103.6
284		44.5	64.7	841	1054	34.0	75.0	.309	42.6	139.7	.0180	1464	2176	301	83	55	79	.266	.262	.0395	623	1121	11.14	103.2
285		43.3	62.8	841	1055	33.9	74.8	.320	43.7	143.3	------	----	----	---	---	-----	-----	-----	-----	------	---	----	11.37	-----
287	Tip peaked	63.6	92.2	584	592	51.1	112.6	.255	31.3	102.6	------	----	----	---	---	-----	-----	-----	-----	------	---	----	6.88	-----
288		63.3	91.9	586	595	51.1	112.7	.257	31.5	103.3	.0132	1092	1506	299	79	66	95	.249	.243	.0651	506	911	7.30	104.2
289	Tip peaked	63.2	91.7	588	598	51.0	112.5	.257	31.6	103.7	.0166	1211	1720	298	77	103	149	.247	.243	.0697	623	1122	7.25	104.4
290		62.9	91.3	588	598	51.2	112.8	.259	31.8	104.5	.0199	1327	1929	298	76	150	218	.290	.286	.0721	739	1331	7.28	104.8
291		63.2	91.7	587	597	50.8	112.1	.256	31.4	103.2	.0217	1385	2033	298	77	178	258	.310	.307	.0718	798	1436	7.25	104.6
294		40.8	59.1	842	1056	34.4	75.8	.339	47.1	154.4	------	----	----	---	---	-----	-----	-----	-----	------	---	----	11.46	-----
295		40.9	59.3	841	1054	34.5	76.0	.339	47.1	154.4	.0096	1184	1671	310	98	15	22	.240	.246	.0463	342	616	11.66	101.7
296	Tip peaked	42.5	61.6	843	1058	34.4	75.8	0.323	45.3	148.7	0.0132	1308	1896	301	82	30	43	0.252	0.246	0.0495	465	837	10.72	102.2
297		42.6	61.7	844	1060	33.3	73.4	.310	43.9	144.1	.0169	1433	2120	302	83	46	68	.255	.250	.0517	589	1060	10.00	103.0
301		42.3	61.3	841	1040	33.3	73.4	.311	44.0	144.5	------	----	----	---	---	-----	-----	-----	-----	------	---	----	9.66	-----
303	Circumferential	62.6	90.9	594	609	51.0	112.4	.256	32.3	106.0	.0132	1093	1507	298	77	64	93	.537	.531	.0482	499	898	7.06	103.9
304		63.0	91.4	594	610	49.9	109.9	.248	31.5	103.2	.0169	1224	1743	298	77	102	148	.498	.494	.0510	630	1134	6.63	104.4
305	Circumferential	62.9	91.3	593	608	49.9	109.9	.249	31.4	103.1	.0204	1344	1959	299	78	152	220	.530	.526	.0502	751	1351	6.83	104.8
308		63.0	91.4	595	611	49.8	109.9	.249	31.5	103.2	------	----	----	---	---	-----	-----	-----	-----	------	---	----	6.38	-----
309		41.9	60.8	843	1058	33.0	72.7	.304	44.3	145.3	.0100	1196	1693	306	91	15	21	.465	.458	.0334	353	635	9.51	101.9
310		41.8	60.6	842	1056	33.9	74.7	.315	45.6	149.5	.0135	1314	1906	302	84	29	42	.477	.471	.0354	473	851	10.20	102.7
311		41.8	60.7	844	1060	33.6	74.1	.313	45.3	148.7	.0151	1369	2005	304	87	37	53	.507	.502	.0366	525	945	10.19	102.7
312	Circumferential	42.1	61.0	843	1057	33.9	74.7	.313	45.3	148.6	.0167	1418	2093	303	85	46	67	.461	.456	.0363	576	1036	10.07	102.7
314		42.0	60.9	846	1064	33.6	74.0	.311	45.2	148.3	------	----	----	---	---	-----	-----	-----	-----	------	---	----	9.50	-----
315	Flat	21.2	30.8	417	292	29.1	64.1	.373	38.2	125.2	------	----	----	---	---	-----	-----	-----	-----	------	---	----	13.14	-----

ditions used in this study. The takeoff condition was simulated except for inlet total pressure, which was reduced due to a facility limitation. The simulated operating conditions are given in table I.

RESULTS AND DISCUSSION

Table II is a list of test results for the takeoff and cruise operating conditions used in the tests. ASTM-A1 fuel was used for all tests. The design average exit temperature of 1478 K (2200° F) was not obtained with all the inlet air velocity profiles due to excessive local temperature peaks which would damage the exit temperature probes. No effort was made to improve the exit temperature distribution.

Inlet Air Velocity Profiles

Four inlet air velocity profiles were used for these tests. Figure 3 shows the flat, center peaked, and tip peaked inlet air velocity profiles where inlet annular height is plotted against the air velocity parameter $(V_{3.5j} - V_{3.5})/V_{3.5}$ for the takeoff and Mach 2.7 cruise conditions. The average velocity at any radius is $V_{3.5j}$ and $V_{3.5}$ is the average velocity of all radii. The slight difference in inlet air velocity parameter between figures 3(a) and (b) at 60 percent of span for the center peaked inlet velocity profile is believed due to a slight distortion of the punched plates used to create the distortion at the higher Mach number for this condition.

The circumferential inlet velocity profile is shown in figure 4. In this figure the inlet air velocity parameter is plotted against circumferential position for each radius measured. Twelve rakes of five points each were used to obtain the profile. Eight rakes were located between the punched plates and the diffuser inlet while the other four rakes were located at the diffuser inlet. For this figure, the $V_{(3 \text{ or } 3.5)j(loc)}$ term in the inlet velocity parameter is the velocity calculated for that particular point, while the $V_{(3 \text{ or } 3.5)j}$ is the average velocity for the twelve pressure tubes at that radius. A more detailed description of these calculations is given in appendix E.

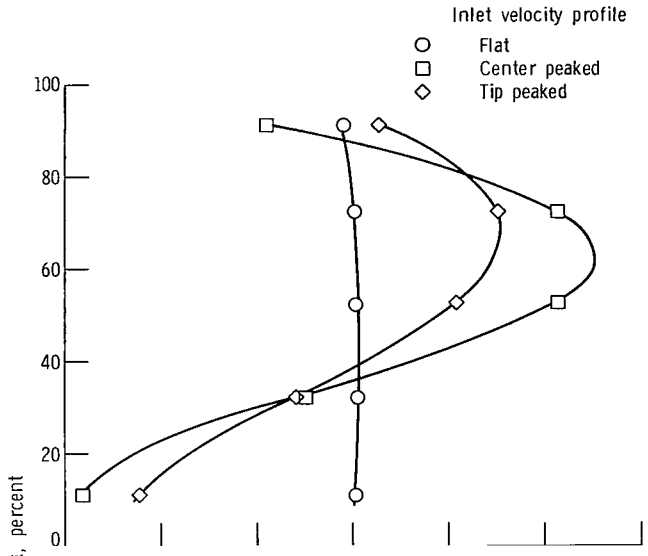

(a) Inlet air condition simulated takeoff. Total pressure, 62 newtons per square centimeter absolute (90 psia); total temperature, 589 K (600° F); reference velocity, 30.5 meters per second (100 ft/sec); average inlet velocity, 115 meters per second (378 ft/sec).

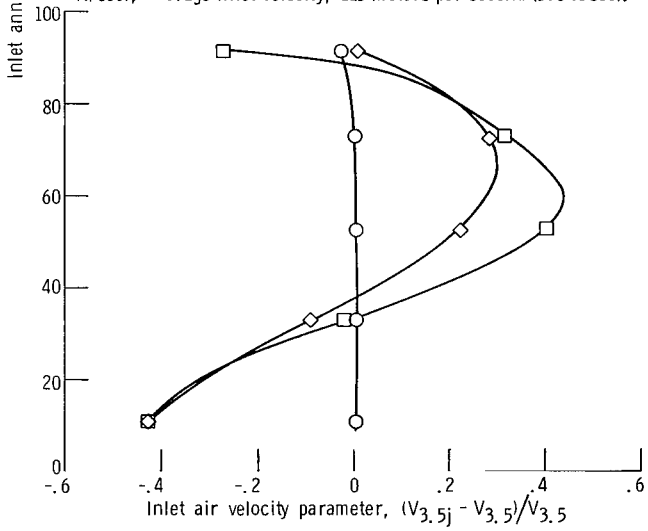

(b) Inlet air condition simulated Mach 2.7 cruise. Total pressure, 41.4 newtons per square centimeter absolute (60 psia); total temperature, 839 K (1050° F); reference velocity, 45.7 meters per second (150 ft/sec); average inlet velocity, 180 meters per second (591 ft/sec).

Figure 3. - Diffuser inlet annulus height plotted against inlet air velocity parameter for flat, center peaked, and tip peaked inlet velocity profiles.

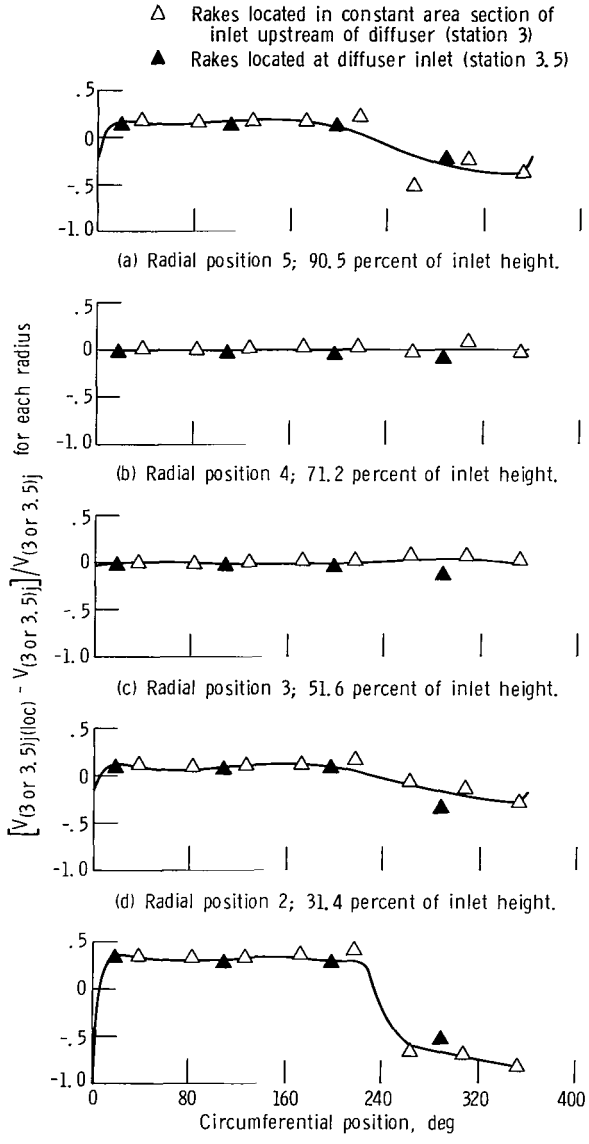

Figure 4. - Inlet air velocity parameter plotted against circumferential position for circumferentially distorted inlet.

TABLE III. - COMBUSTOR SHROUD AIRFLOW SPLITS

Inlet air velocity profile	Flat	Center peaked	Tip peaked
Simulated takeoff[a]			
Percent of inlet flow[b]	83.6	76.8	77.6
Percent flow to outer shroud over total shroud flow	25.5	24.0	27.5
Percent flow to center over total shroud flow	48.9	51.7	50.7
Percent flow to inner shroud over total shroud flow	25.6	24.3	21.8
Simulated Mach 2.7 cruise			
Percent of inlet flow	83.7	74.3	77.0
Percent flow to outer shroud over total shroud flow	25.1	23.0	27.5
Percent flow to center over total shroud flow	48.9	53.2	51.8
Percent flow to inner shroud over total shroud flow	26.1	23.8	20.8

[a]See table I.

[b]Total airflow measured by shroud rakes over diffuser inlet airflow. (Not all airflows through the shroud, some air flows through the head plate and transition liners.)

Airflow Splits

Table III indicates the relative airflow splits between the three airflow passages (outer, center, and inner) indicated in figure 5. These passages are located in the combustor shrouds at the plane of the headplate. Also given in table III is the percentage of inlet air flowing in the three passages. The air that bypasses the three passages enters the combustor through the headplate and transition liners. As can be seen, with a relatively high pressure loss combustor such as this, the airflow is nearly the same for the three passages regardless of inlet velocity profile; that is, 50 percent of the flow to the center passage and 25 percent each to the outer and inner passages. Calculations for determining airflow in the shrouds is given in appendix E.

Pressure Loss

Figure 6 shows combustor pressure loss (which includes the diffuser and combustor pressure loss) as a function of diffuser inlet Mach number for the three distorted inlet

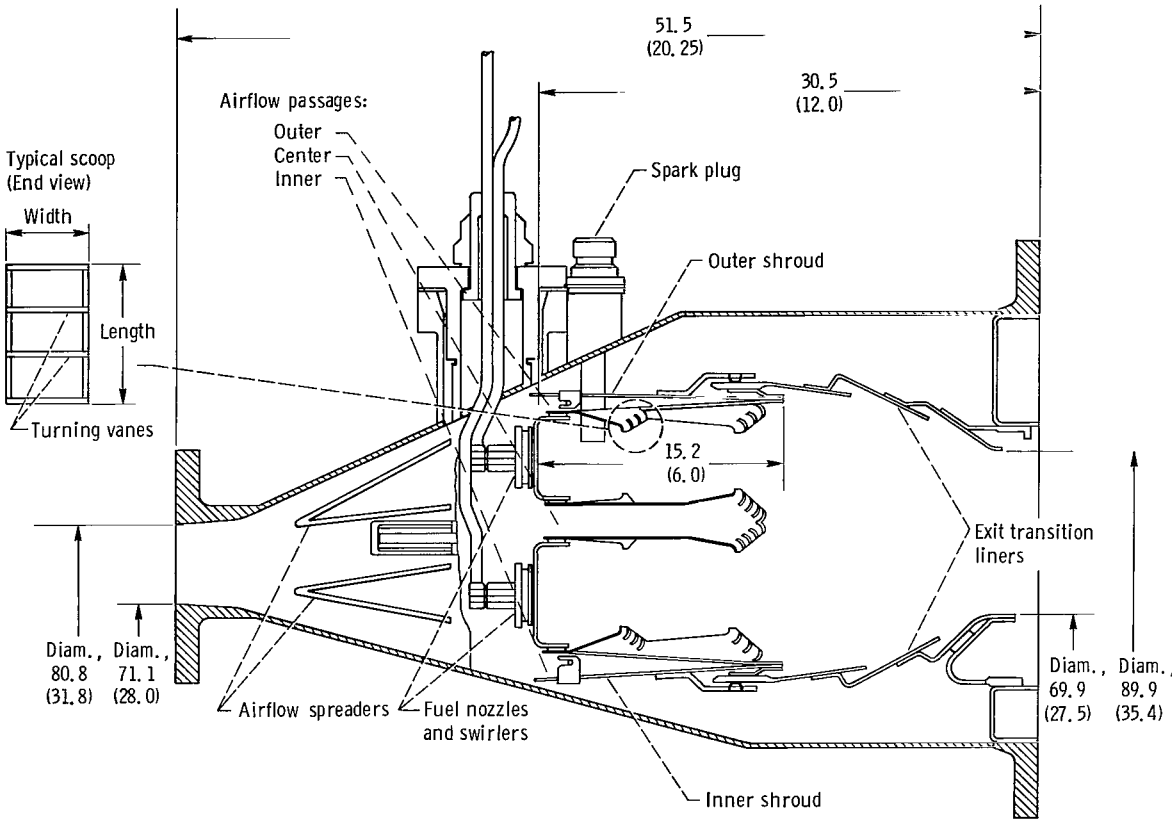

Figure 5. - Cross section of double-annular ram-induction combustor. (All dimensions are in cm (in.).)

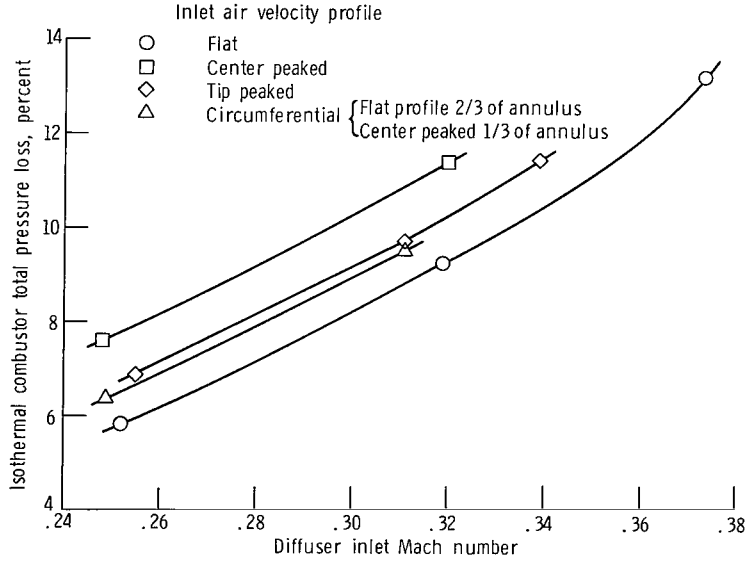

Figure 6. - Isothermal combustor total pressure loss with flat, center peaked, tip peaked, and circumferential inlet air velocity profiles.

velocity profiles and the flat profile. The distorted profiles increased the pressure loss up to 2 percentage points above the flat profile's pressure loss. The higher pressure losses observed with the various profiles may be due to turning losses in the diffuser caused by the distorted air channeling back into the three flow passages. The increase in pressure loss with circumferentially distorted profile was one-third of the increase in pressure loss observed with the center peaked profile compared to the flat inlet profile. Also, the increase in pressure loss of the tip peaked profile was one-half of the increase in pressure loss of the center peaked profile compared to the flat inlet profile. Both observations are to be expected. The first because one-third of the annulus saw a center peaked profile while the rest saw the flat profile. The second observation was expected because the blockage plates used in the center peaked case were of nearly equal area, thus if one were removed about half the loss in pressure over a flat profile should be recovered.

Radial Temperature Profile

The design temperature profile at the combustor exit plane is determined by the stress and cooling characteristics of the turbine in a particular engine application. For the purpose of evaluating the combustor, a design exit average radial temperature profile typical of advanced engines was selected. The measured exit average radial temperature profiles for the different inlet air velocity profiles is compared with the design temperature profile in figure 7. The open symbols indicate the exit average temperatures measured at each radial position. Also shown are the maximum temperature deviations at each radial position measured at any point around the circumference (solid symbols). The effect of the various inlet air profiles on the average radial temperature profile was small. The largest difference in average radial temperature between actual and desired was 43 K (77° F) which occurred at the radius nearest the hub. The largest difference in maximum temperature values between profiles excluding the circumferential inlet air velocity profile was only 54 K (97° F) occurring at the center radius. An explanation of the high maximum temperatures of the circumferential inlet air velocity profile is given in the Circumferential Temperature Profile section.

As would be expected from the slight increase in airflow to the outer airflow passage with the tip peaked inlet air velocity profile (see fig. 3 and table III), the exit temperatures near the tip are cooler and the exit temperatures near the hub are warmer than with the other inlet air velocity profiles. The similar results on average radial temperature profiles obtained with the various inlet air velocity profiles are due to the nearly identical air distribution between the airflow passages for the different inlet air velocity profiles.

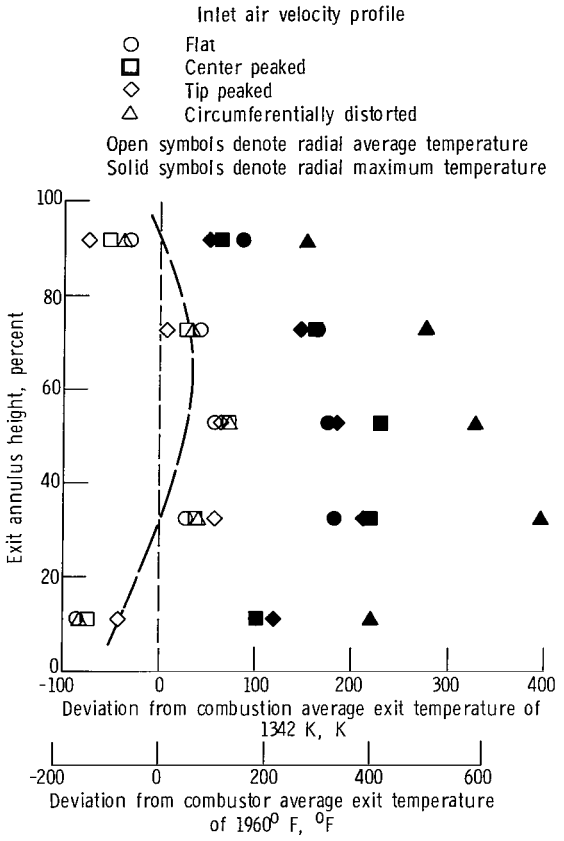

Figure 7. - Variation of exit average radial temperature profile with inlet air velocity profile. Simulated takeoff air condition: total pressure, 62 newtons per square centimeter absolute (90 psia); total temperature, 589 K (600° F); reference velocity, 30.5 meters per second (100 ft/sec).

Combustor Exit Temperature Distribution Parameters

Figure 8 is a comparison of pattern factor, stator factor, and rotor factor plotted against combustor average temperature rise for the two airflow conditions and the various inlet air velocity profiles tested. As can be seen in figures 8(a) and (b), the pattern factors and stator factors ranged from 0.19 to 0.32 for the two airflow ranges and inlet air velocity profiles tested (excluding the circumferential distorted profile). The best pattern and stator factors were observed with the flat inlet air velocity profile and ranged from 0.19 to 0.27. The stator factor and pattern factor for the circumferential inlet air velocity profile ranged from 0.46 to 0.54. This particularly poor performance is explained in the Circumferential Temperature Profile section.

Rotor factor varied from 0.0385 to 0.0845 at the 589 K (600° F) inlet air condition and varied from 0.0215 to 0.052 at the 839 K (1050° F) inlet air condition regardless of

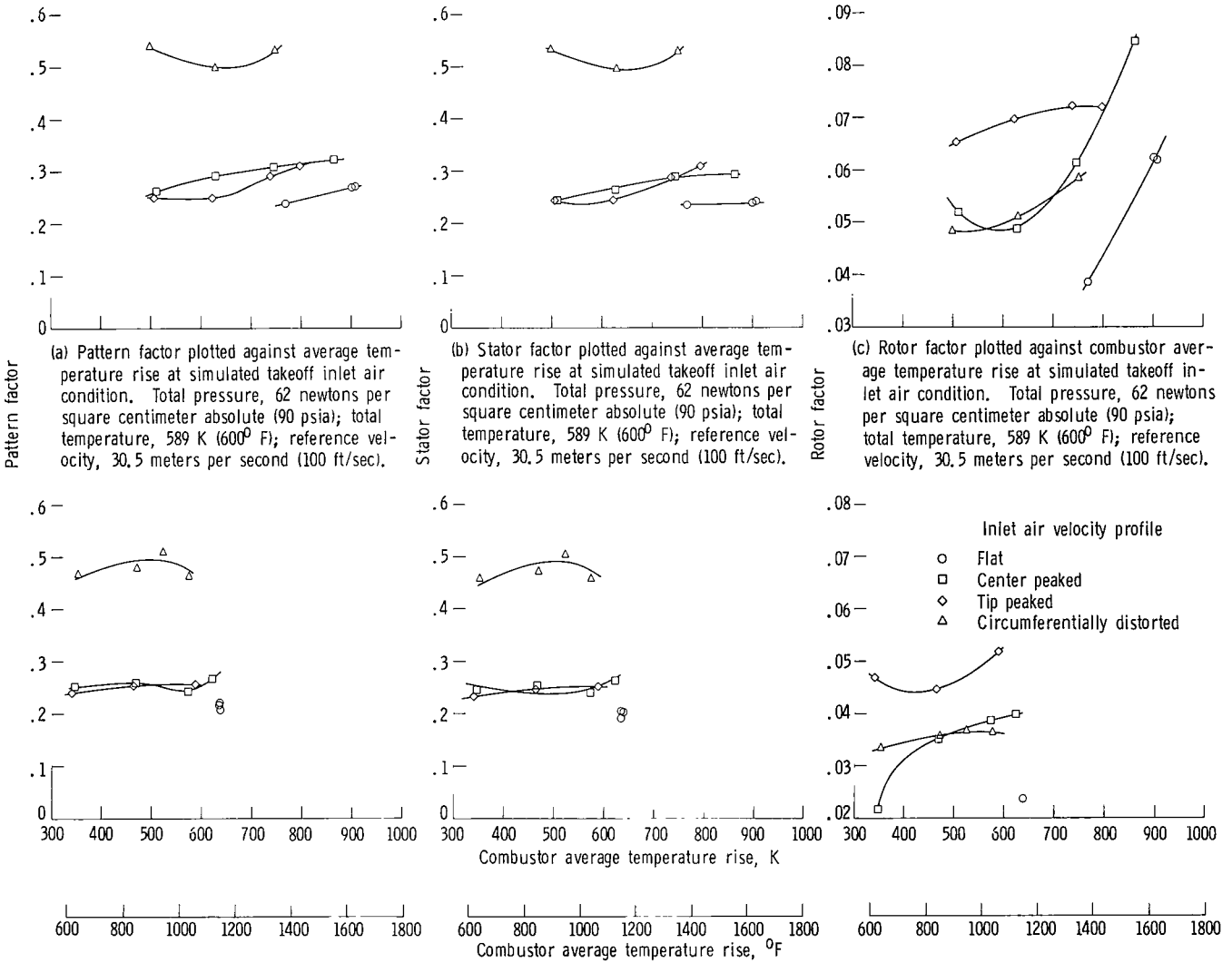

(a) Pattern factor plotted against average temperature rise at simulated takeoff inlet air condition. Total pressure, 62 newtons per square centimeter absolute (90 psia); total temperature, 589 K (600° F); reference velocity, 30.5 meters per second (100 ft/sec).

(b) Stator factor plotted against average temperature rise at simulated takeoff inlet air condition. Total pressure, 62 newtons per square centimeter absolute (90 psia); total temperature, 589 K (600° F); reference velocity, 30.5 meters per second (100 ft/sec).

(c) Rotor factor plotted against combustor average temperature rise at simulated takeoff inlet air condition. Total pressure, 62 newtons per square centimeter absolute (90 psia); total temperature, 589 K (600° F); reference velocity, 30.5 meters per second (100 ft/sec).

(d) Pattern factor plotted against combustor average temperature rise at simulated Mach 2.7 cruise air condition. Total pressure, 41.4 newtons per square centimeter absolute (60 psia); total temperature, 839 K (1050° F); reference velocity, 45.7 meters per second (150 ft/sec).

(e) Stator factor plotted against combustor average temperature rise at simulated Mach 2.7 cruise air condition. Total pressure, 41.4 newtons per square centimeter absolute (60 psia); total temperature, 839 K (1050° F); reference velocity, 45.7 meters per second (150 ft/sec).

(f) Rotor factor plotted against combustor average temperature rise at simulated Mach 2.7 cruise air condition. Total pressure, 41.4 newtons per square centimeter absolute (60 psia); total temperature, 839 K (1050° F); reference velocity, 45.7 meters per second (150 ft/sec).

Figure 8. - Comparison of pattern factor, stator factor, and rotor factor plotted against combustor average temperature rise.

inlet air velocity profile. Rotor factor with the circumferential inlet air velocity profile was not the worst case as it was with pattern and stator factor.

Circumferential Temperature Profile

Figure 9 shows the circumferential variation of exit temperature. The temperatures shown are averages of the five radial temperature measurements at any one circumferential position. Data were taken every 3° around the circumference. These data were obtained at the simulated takeoff condition of table I. As would be expected from the pattern factor and stator factor data, there is little difference between figures 9(a) to (c) representing the flat, center peaked, and tip peaked profiles, respectively. Note that the exit average temperature varies somewhat between figures 9(a) to (c).

Figure 9(d) presents the circumferential temperature profile for the circumferentially distorted inlet velocity profile. Note there is a definite increase in circumferential average temperature in the 246° to 360° and 0° to 6° circumferential regions which are directly downstream of the inlet blockage plates. As less air flows in this region due to the blockage plates compared to the unblocked region and the same fuel flow per fuel nozzle was introduced in both regions, a higher local fuel-air ratio and hence temperature resulted in the blocked region. This increased the pattern factor and stator factor even with no increase in temperature deviation from the average temperature in each region. This occurs because the $(T_{max} - T_{av})$ term is inflated by the difference between the blocked region's average temperature and the overall average temperature. This effect is illustrated in appendix E in the section entitled Exit Temperature Profiles. If in figure 7(d), the pattern factor had been computed using the average temperature which occurred in the region downstream of the blockage plates, the pattern factor would drop to 0.34. This compares to a pattern factor of 0.32 in figure 8(a), for the center peaked inlet velocity profile at the same temperature rise that was observed in the hot section of figure 9(d). In a similar manner, the stator factor would change from 0.53 to 0.34 compared to 0.29 for the center peaked inlet velocity profile. Similarly rotor factor would change from 0.058 to 0.092 compared to 0.083 for the center peaked inlet velocity profile.

The circumferential temperature profiles have not been plotted for the cruise condition (table I) as the combustor average temperature rises for the various inlet air velocity profiles were less than with the takeoff condition. Thus, only the more severe point has been presented.

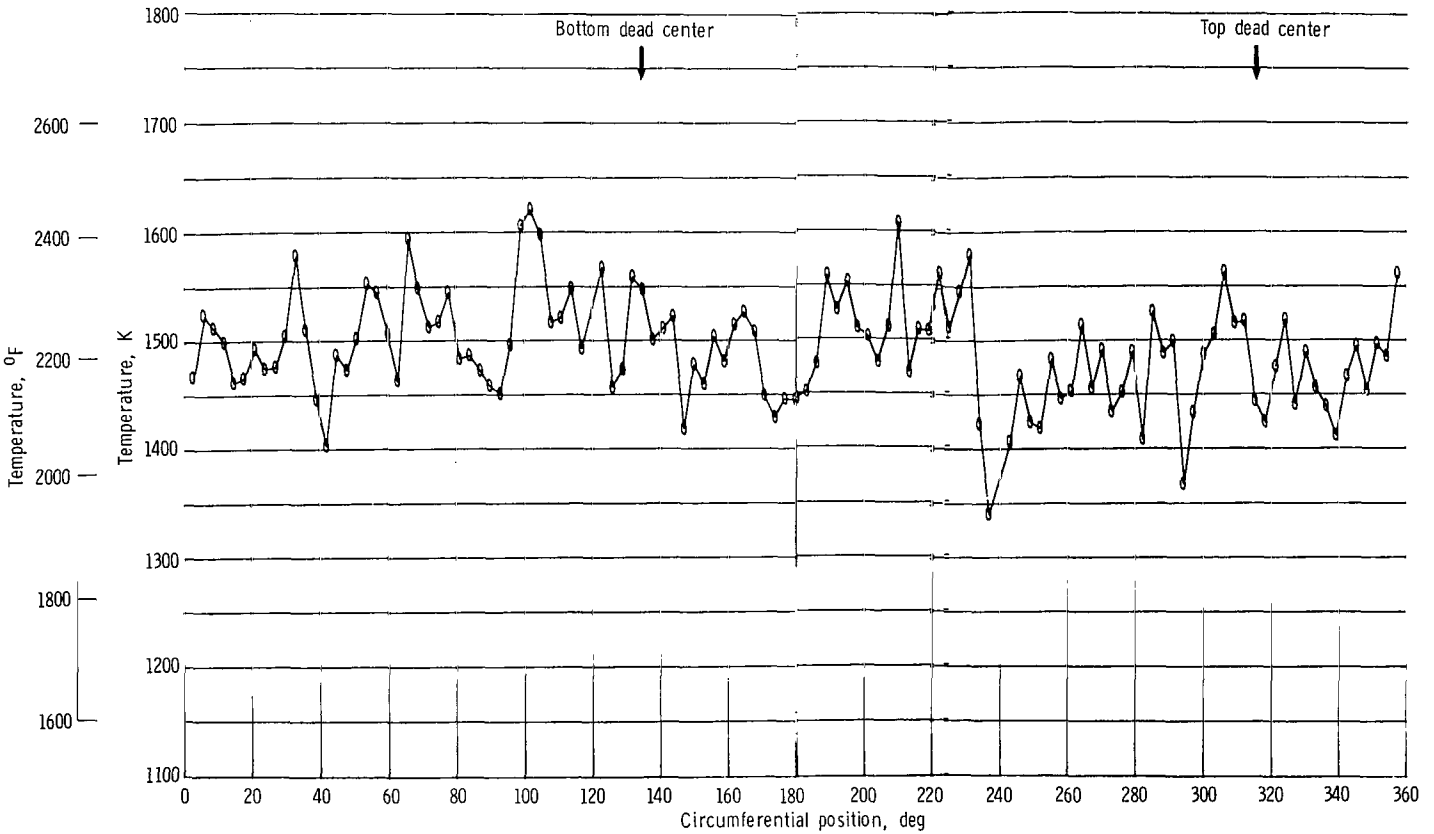

(a) Flat inlet velocity profile.

Figure 9. - Radial average temperature plotted against circumferential position at simulated takeoff air condition. Total pressure, 62 newtons per square centimeter absolute (90 psia); total temperature, 589 K (600° F); reference velocity, 30.5 meters per second (100 ft/sec).

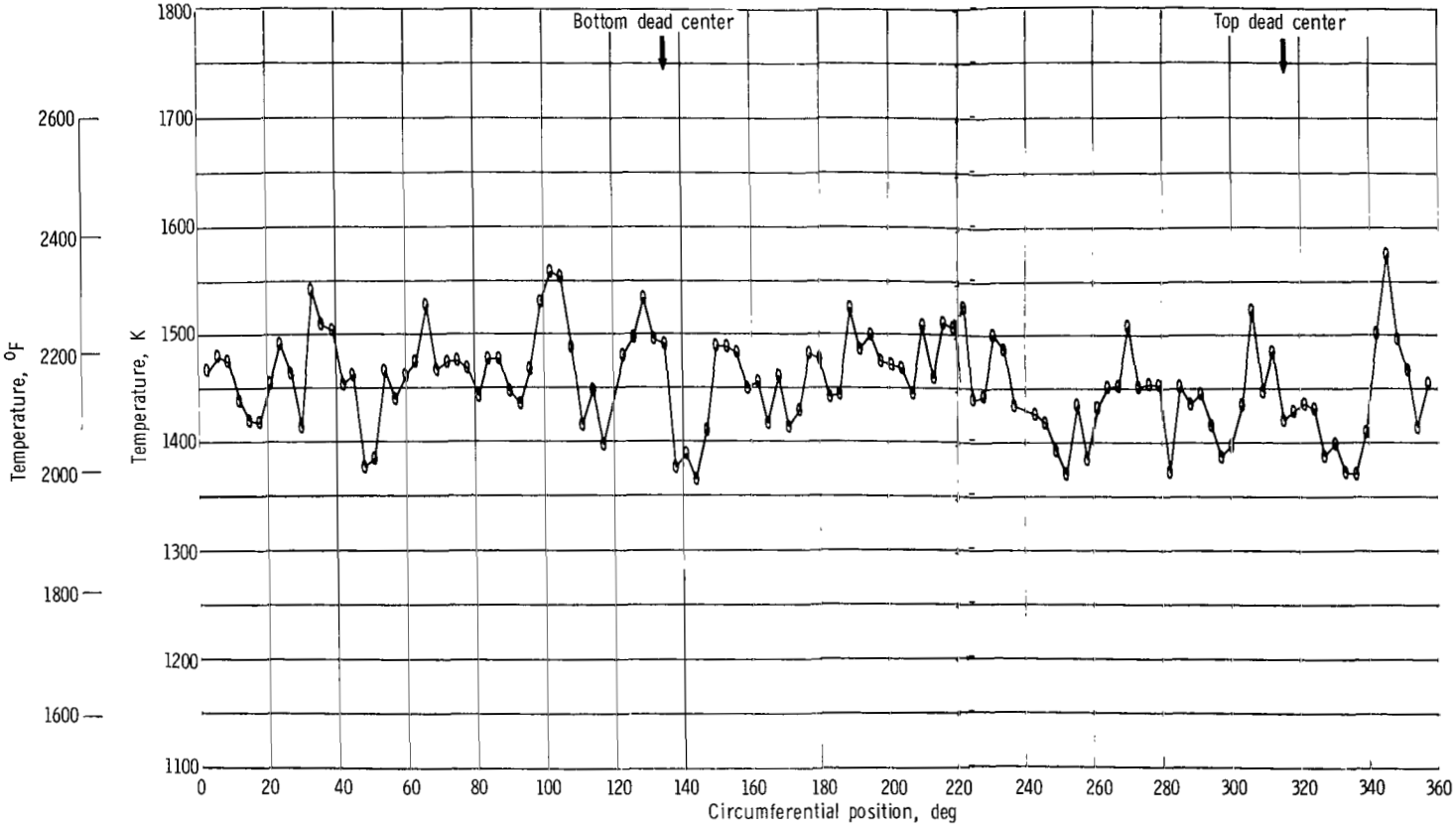

(b) Center peaked inlet velocity profile.

Figure 9. - Continued.

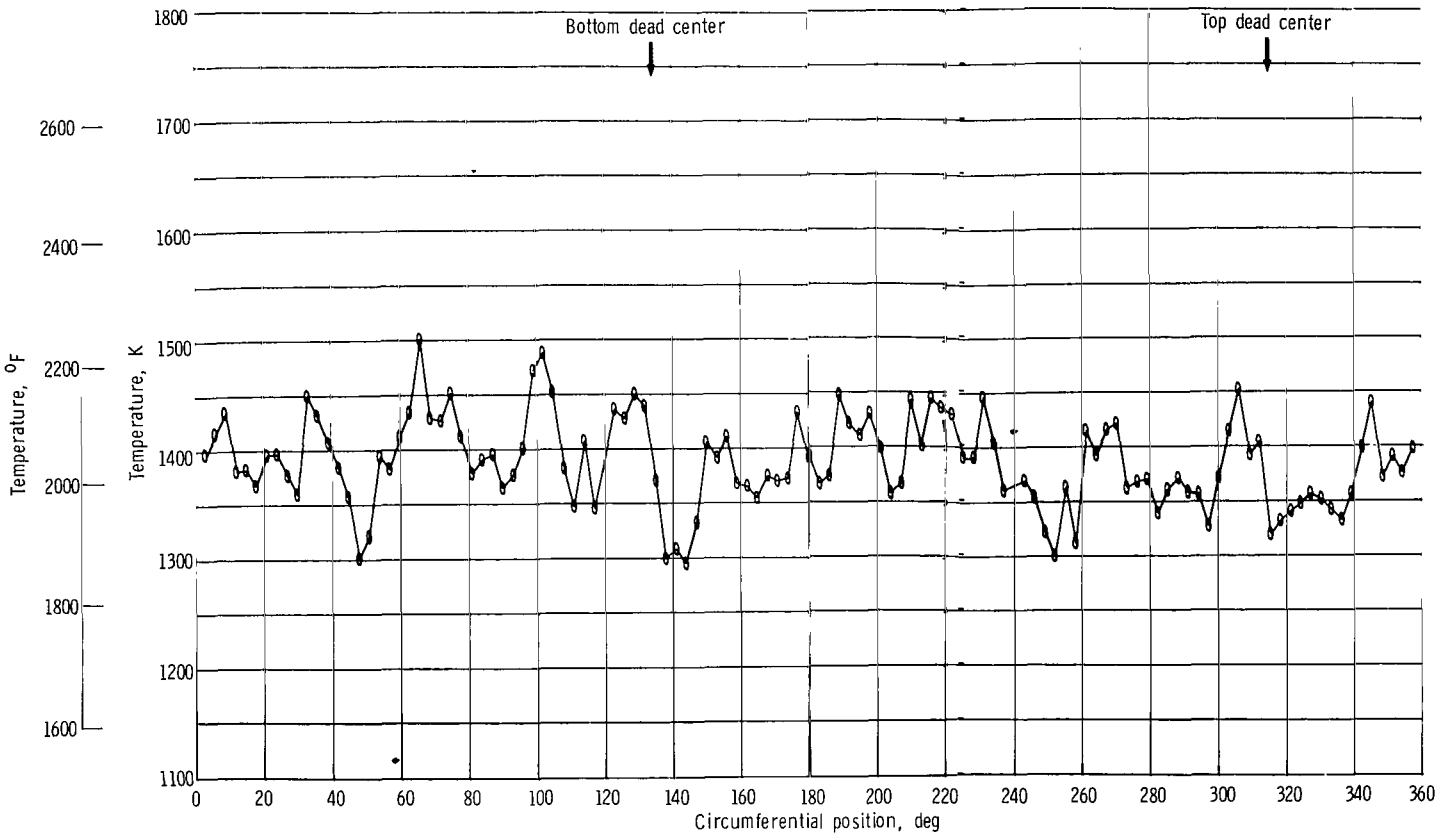

(c) Tip peaked inlet velocity profile.

Figure 9. - Continued.

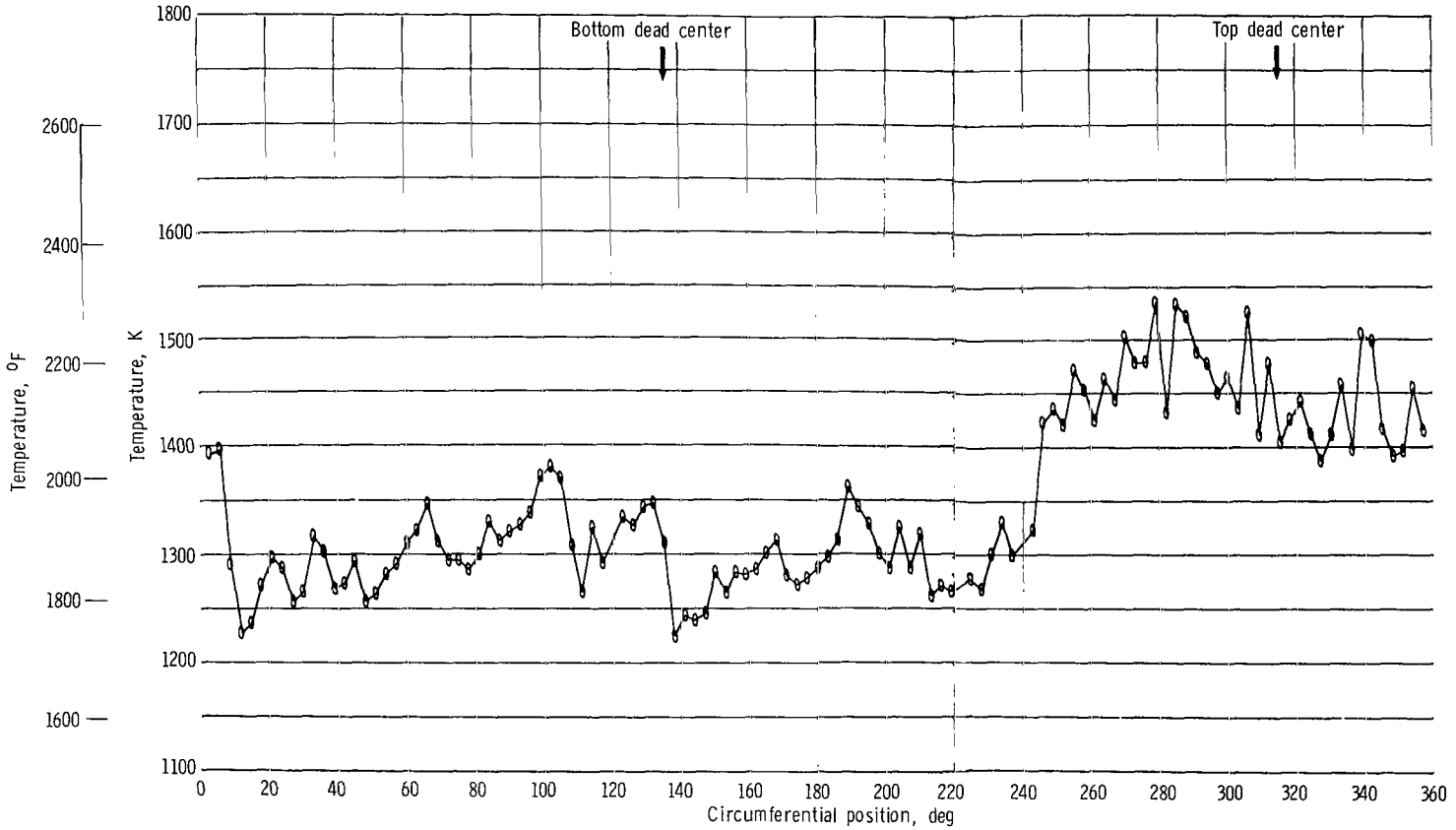

(d) Circumferentially distorted inlet velocity profile.

Figure 9. - Concluded.

Combustion Efficiency

Inlet air velocity profile, flat or radially and circumferentially distorted, had no effect on combustion efficiency. Combustion efficiency was 100 percent for both the simulated takeoff and Mach 2.7 cruise conditions.

SUMMARY OF RESULTS

Full-scale tests were conducted on a short-length double-annular ram-induction combustor to determine the effects of distorted diffuser inlet velocity profiles on performance. Both radial and circumferential distortions were used in the evaluation. Previous tests of this combustor with flat inlet profiles showed satisfactory performance comparable to similar annular combustors about 50 percent longer.

The following results with distorted inlet profiles at both simulated sea-level takeoff and Mach 2.7 cruise conditions were obtained:

1. With the exception of the circumferentially distorted inlet velocity profile, the exit radial temperature profile was unaffected by inlet air profile distortions.

2. Pattern and stator factors were unaffected by radially distorted inlet velocity profiles and ranged from 0.19 to 0.32.

3. The circumferentially distorted inlet velocity profile doubled pattern and stator factors compared to the flat profile resulting in valves of 0.46 to 0.54.

4. Rotor factor was unaffected by inlet velocity profile, either radial or circumferential, and ranged from 0.0385 to 0.0845 at simulated takeoff and from 0.0215 to 0.052 at simulated Mach 2.7 cruise condition.

5. Distorted inlet air profiles increased the pressure loss up to two percentage points above that for the flat inlet profile. A flat inlet air velocity profile with a diffuser inlet Mach number of 0.3 produced a total pressure loss from diffuser inlet to combustor exit of 8.2 percent.

6. With this relatively high pressure loss combustor, airflow redistributes itself in the diffuser to obtain approximately the same airflow split between combustor passages regardless of the inlet air velocity profiles.

7. Combustion efficiency was 100 percent for all conditions tested.

CONCLUDING REMARKS

In all, the different inlet air velocity profiles had little effect on combustor performance except the circumferential distorted velocity profile. All the profiles in-

creased the combustor pressure loss compared to the undistorted conditions. In addition, the circumferentially distorted velocity profile significantly increased the combustor pattern and stator factors. The effect on exit temperature of circumferentially distorted velocity profiles like radially distorted velocity profiles would probably remain as severe or become more severe with a lower pressure loss combustor.

Exit temperature distortions induced by radial inlet air velocity profiles can often be corrected by minor changes in combustor hardware. Such changes as varying the fuel flow split between annuli in multiple annuli combustors, changing the fuel nozzle spray angle, and adding, blocking, or moving holes or slots in the combustor liners fall in this category. It is unlikely, however, that a circumferentially distorted inlet velocity profile can be corrected with minor combustor hardware changes.

Lewis Research Center,
National Aeronautics and Space Administration,
Cleveland, Ohio, December 6, 1971,
764-74.

APPENDIX A

SYMBOLS

P	pressure
ΔP	total pressure drop across combustor, $P_{t3} - P_{t4}$
T	temperature
ΔT	temperature rise across combustor, $T_{t4} - T_{t3}$
V	velocity
$\overline{\delta}$	pattern factor
δ_{rot}	rotor factor
δ_{stat}	stator factor
$\theta_0, \theta_1, \theta_2$	circumferential positions

Subscripts:

av	average
des	design
j	radial location
loc	local (a single point)
max	maximum (a single point)
ref	reference
s	static
t	total
3	11.4-cm (4.5-in.) upstream of diffuser inlet
3.5	diffuser inlet
4	combustor exit

APPENDIX B

COMBUSTION DESIGN

The Double-Annular Concept

The combustor used in this investigation is referred to as a double-annular ram-induction combustor. Constructing the combustion zone as a double annulus permits the reduction of overall combustor length while maintaining an adequate ratio of length to annulus height in each combustion zone. This double-annular feature allows a considerable reduction in length to be made over a single annulus with the same overall height.

However, individual control of the inner and outer annulus fuel systems of the double-annular combustion zone provides a useful method for adjusting the outlet radial temperature profile.

The Ram-Induction Concept

The ram-induction combustor differs from the more conventional combustors in that the compressor discharge air is allowed to penetrate into the combustion and mixing zones without diffusing to as high a static pressure as a conventional static pressure-fed combustor. The kinetic energy of the inlet air is thereby used to promote rapid mixing of air and fuel in the primary zone and diluent air and burned gases in the mixing zone. The airflow is efficiently turned into the combustor by two rows of vaned turning scoops that penetrate into the combustion zones.

The ram-induction combustor has several advantages over conventional static pressure-fed combustors; they are the following:

(1) A shorter length combustor is obtained because more controlled mixing can be established in the combustion zone. This is achieved by better control of the airflow injection angle with the vaned turning scoops.

(2) Diffuser length can be shortened since diffusion to very low combustor air velocities is no longer needed or desired. The overall diffuser-combustor length can, therefore, be reduced. The small area ratio diffuser in the shorter length could have less pressure loss since it is not as prone to flow separation as combustors of larger area ratios. However, this advantage can be offset by the increased turning losses associated with spreading the relatively high velocity flow evenly into the combustor.

(3) The high velocity flow over the exterior surfaces of the combustor provides substantial convective cooling of these walls. This reduces the film cooling air requirements. Thus more air is available for mixing and temperature profile control.

A more detailed discussion of the ram-induction concept is provided in reference 4.

Combustor Design Details

The double-annular ram-induction combustor including the diffuser section used for this investigation is shown in cross section in figure 5. Forward airflow spreaders in the diffuser split the inlet airflow into three passages leading into the combustor. These are the inner liner passage, the outer liner passage, and the center passage. About 50 percent of the airflow is ducted by shrouds surrounding the outside of both the outer and inner liners of the combustors. The high velocity airflow which is maintained from the diffuser inlet through this ducting is turned into the combustor burning zones by means of the scoops discussed previously. The first row of scoops supplies air to the primary zone while the second row supplies diluent air to the secondary zone.

Basic dimensions for this combustor are shown in figure 5. The diameters are essentially those of the combustor for the Pratt and Whitney Aircraft experimental supersonic transport engine (JTF 17 (ref. 5)). However, the diffuser-combustor overall length of the double-annular combustor is about 30 percent shorter than that used in the JTF 17 engine.

Photographs of the combustor are shown in figure 10. Figure 10(a) shows the downstream end with the two circumferential rows of scoops of the inner and outer liners and those of the center section. Figure 10(b) is a closeup of this same view showing more detail of the scoop arrangement. The fuel nozzles and associated swirlers are removed, but the deflectors for cooling the inner and outer headplates are shown at the nozzle locations. A side view of the combustor with the upstream diffuser airflow spreaders and inner exit transition liner added to the combustor is shown in figure 10(c). The notches in the airflow spreaders fit around the diffuser struts. The combustor is pin mounted through the struts using tangs attached to the inner and outer headplates that extend forward into the airflow spreaders.

Fuel nozzles. - Simplex fuel nozzles with air swirlers were used for the investigation. A curve of total fuel flow for the combustor (sum of 64 nozzles) as a function of pressure drop across these nozzles are shown in figure 11.

Combustor design specifications. - The major items in the combustor design are tabulated in table IV. The circumferential locations of combustor components such as scoops, fuel nozzles, and diffuser struts are shown in figure 12. The flow areas as distributed among the many openings (scoops, film cooling, swirlers, etc.) are given on the combustor sketch of figure 13. The scoop discharge areas with length and width dimensions are listed in table V.

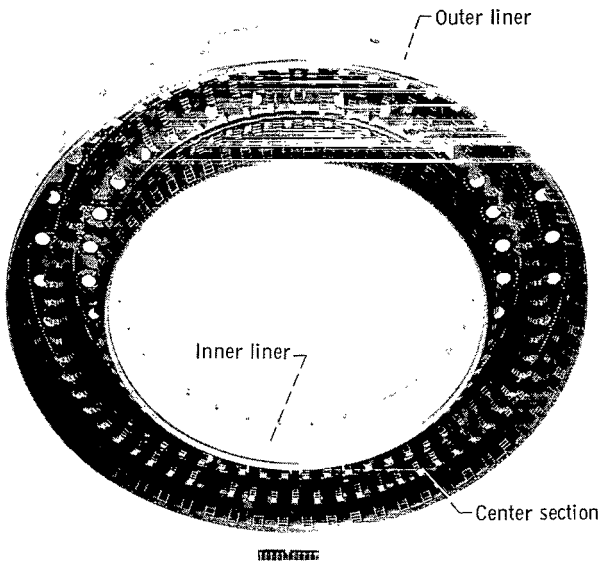

C-68-3605

(a) Viewed from downstream (fuel nozzles removed).

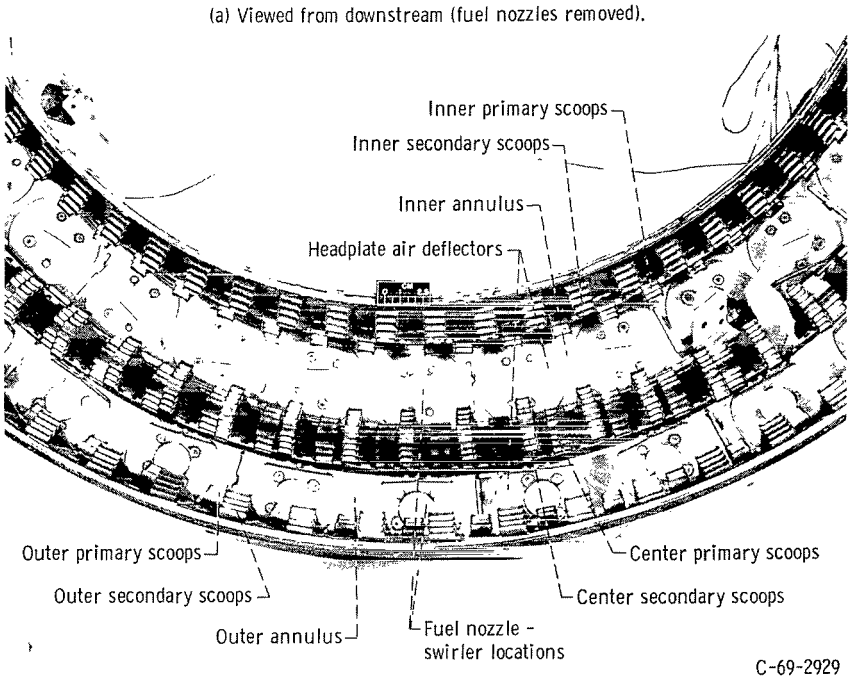

C-69-2929

(b) Closeup view.

Figure 10. - Double-annular ram-induction combustor.

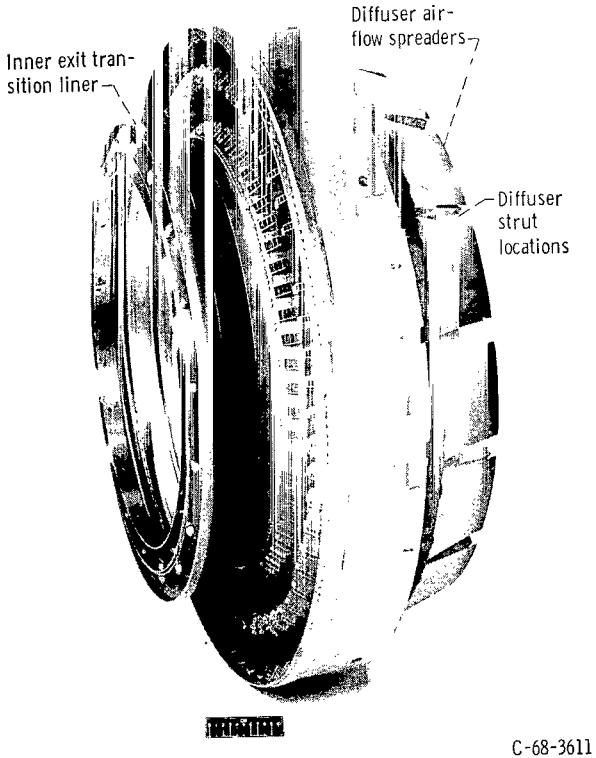

(c) Side view (outer transition liner removed).

Figure 10. - Concluded.

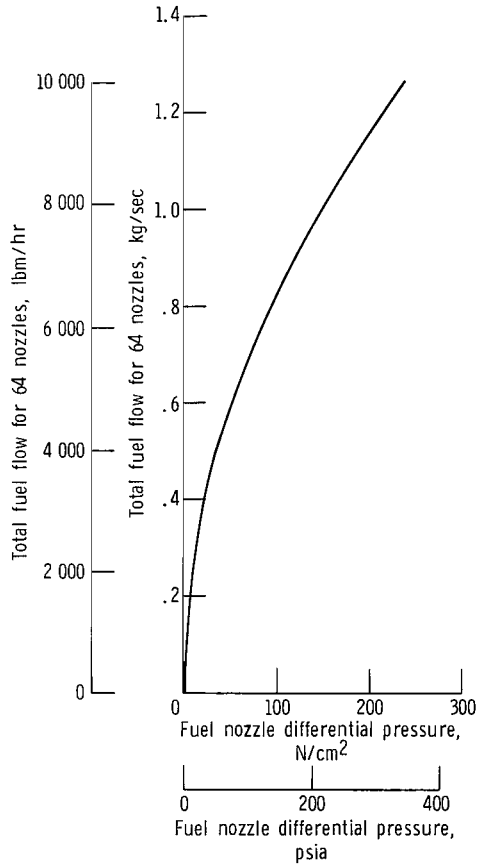

Figure 11. - Fuel flow as function of pressure drop across fuel nozzles of double-annular combustor.

TABLE IV. - DOUBLE-ANNULAR RAM-INDUCTION COMBUSTOR DIMENSIONS AND SPECIFICATIONS

Lengths	
Compressor exit to turbine inlet, cm (in.)	51.5 (20.25)
Fuel nozzle face to turbine inlet, cm (in.)	30.5 (12.00)
Diameters	
Inlet outside diameter, cm (in.)	80.77 (31.80)
Inlet inside diameter, cm (in.)	71.1 (28.00)
Outlet outside diameter, cm (in.)	89.9 (35.38)
Outlet inside diameter, cm (in.)	69.9 (27.50)
Shroud	
Outside diameter, cm (in.)	94.2 (37.09)
Inside diameter, cm (in.)	57.2 (22.52)
Reference area (between shrouds), cm^2 ($in.^2$)	4270 (663)
Diffuser inlet area, cm^2 ($in.^2$)	1177 (182.5)
Open hole area (including cooling), cm^2 ($in.^2$)	1291 (200)
Flow spreader inlet areas	
Outside diameter passage, cm^2 ($in.^2$)	348 (54.0)
Center passage, cm^2 ($in.^2$)	785 (121.5)
Inside diameter passage, cm^2 ($in.^2$)	339 (52.5)
Exit area, cm^2 ($in.^2$)	2503 (388)
Number of fuel nozzles and swirlers	64
Number of diffuser struts	16
Number of ram-induction scoops	512
Rows, primary zone	1
Rows, secondary zone	1
Ratio length to annulus height	
Outer annulus	4.8
Inner annulus	3.9

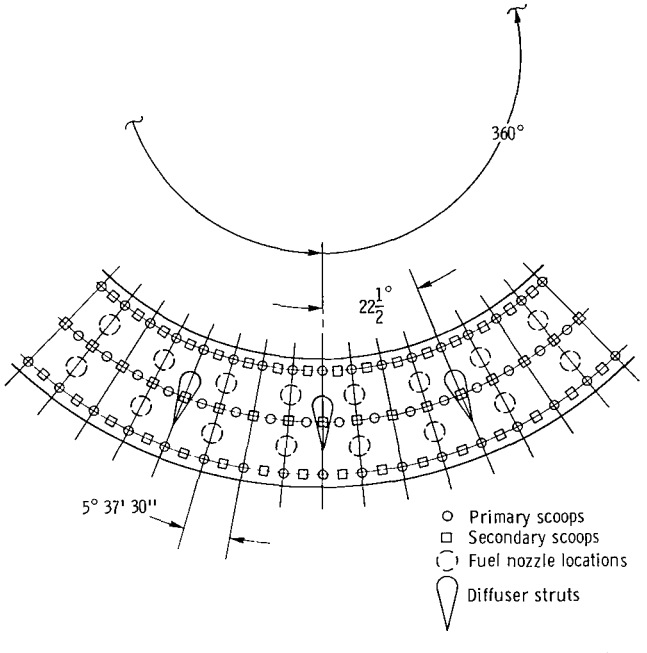

Figure 12. - Circumferential arrangement of combustor scoops and fuel nozzles.

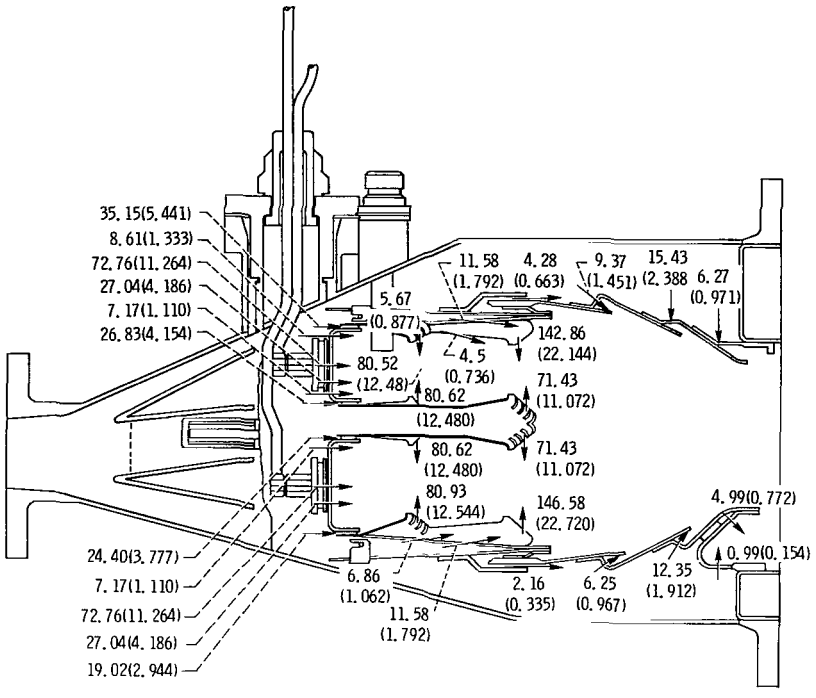

Figure 13. - Effective flow area distribution for double-annular ram-induction combustor. Swirler discharge coefficient, 0.50; hole discharge coefficient, 0.62; scoops and slot discharge coefficient, 1.00; total area (effective), 1184.547 square centimeters (183.374 in.^{2}). (All areas are based on a full annulus with units of cm^2 in.^{2}).)

TABLE V. - SCOOP AREAS[a] AND SIZES FOR DOUBLE-ANNULAR RAM-INDUCTION COMBUSTOR[b]

Type of scoop	Discharge area		Length		Width	
	cm^2	in.^{2}	cm	in.	cm	in.
Outer liner primary	80.516	12.480	1.163	0.458	1.163	0.458
Outer liner secondary	142.864	22.144	1.560	.614	1.560	.614
Outer center shroud primary	80.516	12.480	1.163	.458	1.163	.458
Outer center shroud secondary	71.432	11.072	1.560	.614	.803	.306
Inner center shroud primary	80.516	12.480	1.163	.458	1.163	.458
Inner center shroud secondary	71.432	11.072	1.560	.614	.803	.306
Inner liner primary	80.929	12.544	1.222	.481	1.112	.438
Inner liner secondary	146.580	22.720	1.963	.773	1.245	.490

[a]All areas are actual area for full annulus.

[b]See fig. 1.

APPENDIX C

TEST FACILITY

The full-scale double-annular ram-induction combustor investigation was conducted in a closed-duct test facility of the Engine Components Research Laboratory at Lewis. A sketch of this facility is shown in figure 14. Airflows for combustion up to 136 kilograms per second (300 lbm/sec) at pressures from below atmospheric to 10 atmospheres could be heated to 922 K (1200° F) without vitiation before entering the combustor under test.

For combustor inlet air temperatures of 589 K (600° F) or less, an indirect-fired heat exchanger was used. For higher inlet temperatures (to 922 K (1200° F)), a second stage of indirect heating was used. Heat for the second stage was provided by a natural-gas-fueled J-57 jet engine with an afterburner. The engine exhaust gases were passed through a heat exchanger of special design shown in figure 15.

Figure 16 shows the combustor test section and the connected inlet and outlet ducting. About $4\frac{1}{2}$ pipe diameters of constant area duct was ahead of the test section, which included the diffuser inlet and diffuser as part of the housing. The combustor housing measured 1.0 meters (40 in.) at the maximum diameter and was 0.96 meter (38 in.) long including the inlet section. Following the combustor housing was the outlet instrumentation section. Downstream of this section, the combustor exhaust gases were cooled by a water-injection spray system. The exposed surfaces downstream of the combustor were cooled by two methods: (1) circulating water in passages adjacent to the hot surfaces, and (2) water sprays impinging directly on the exposed surfaces. Photographs of the test section installation are shown in figure 17.

Airflow rates and combustor pressures were regulated by remotely controlled valves upstream and downstream of the test section. Flow straighteners were used to evenly distribute the airflow entering the combustor (see figs. 14 and 16).

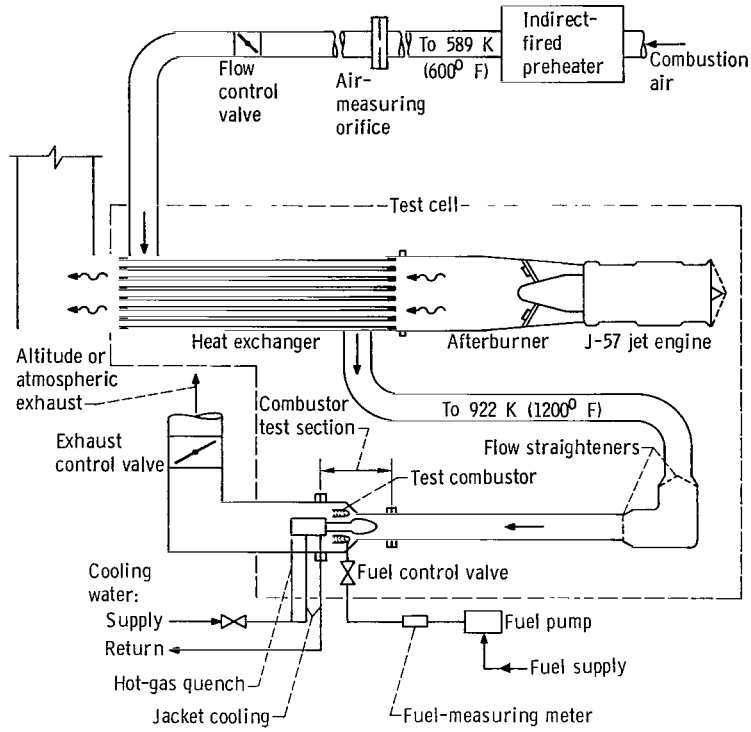

Figure 14. - Test facility and associated systems for full-scale advanced annular combustor tests.

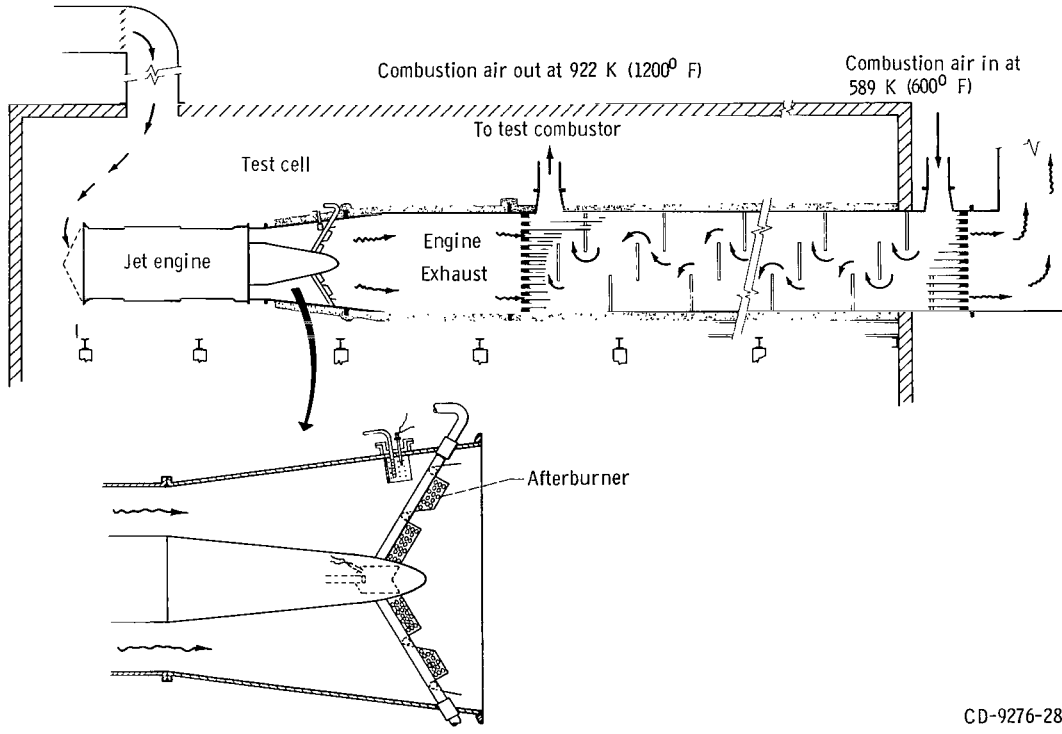

Figure 15. - Heat exchanger in exhaust of jet engine to provide high-temperature inlet air for test combustor.

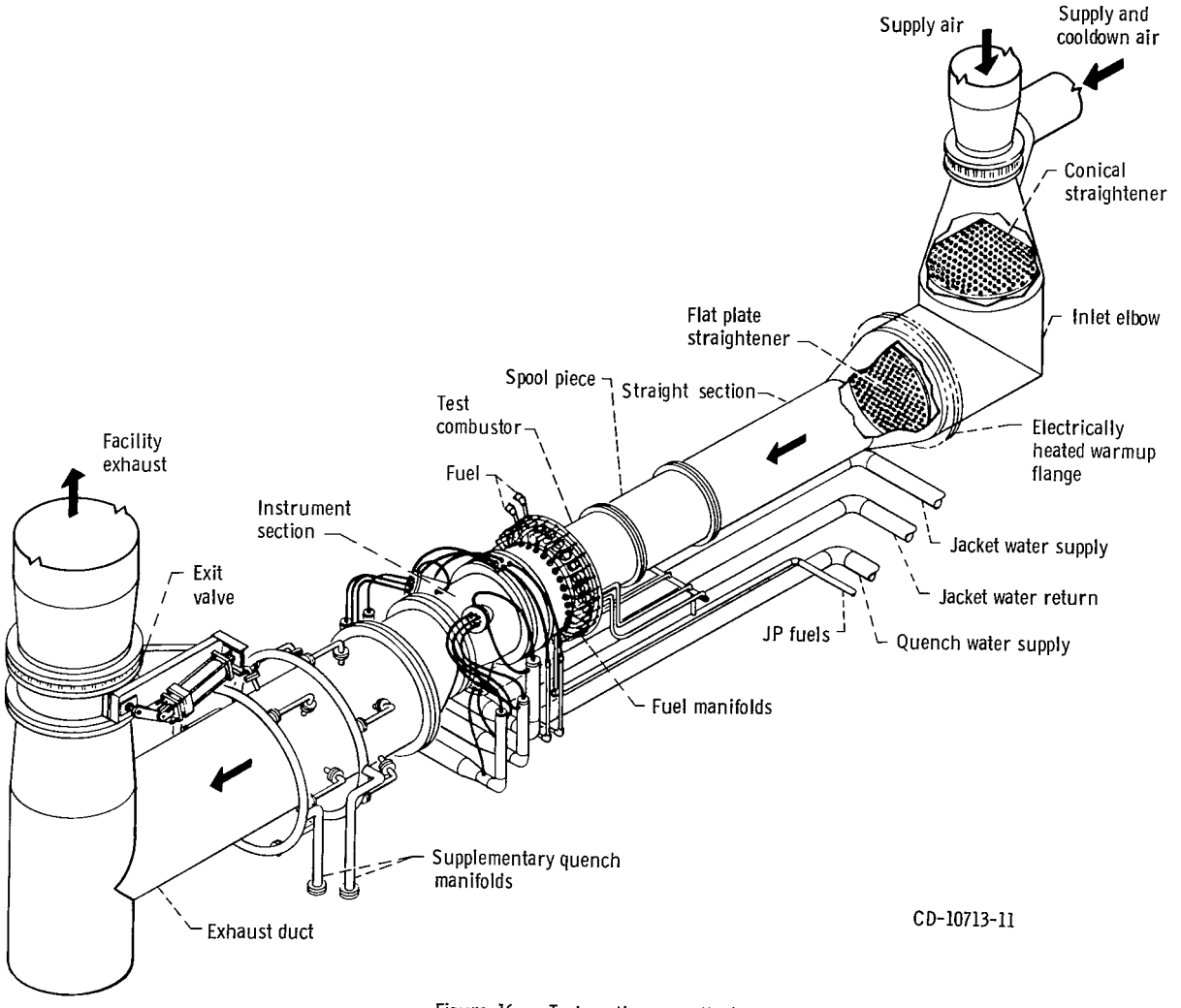

Figure 16. - Test section overall view.

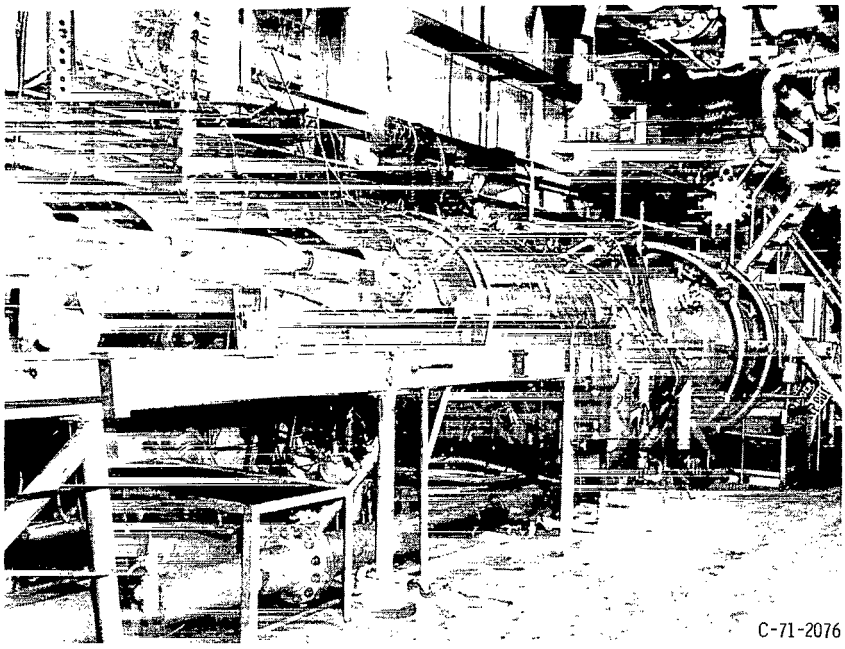

(a) Overall view looking downstream.

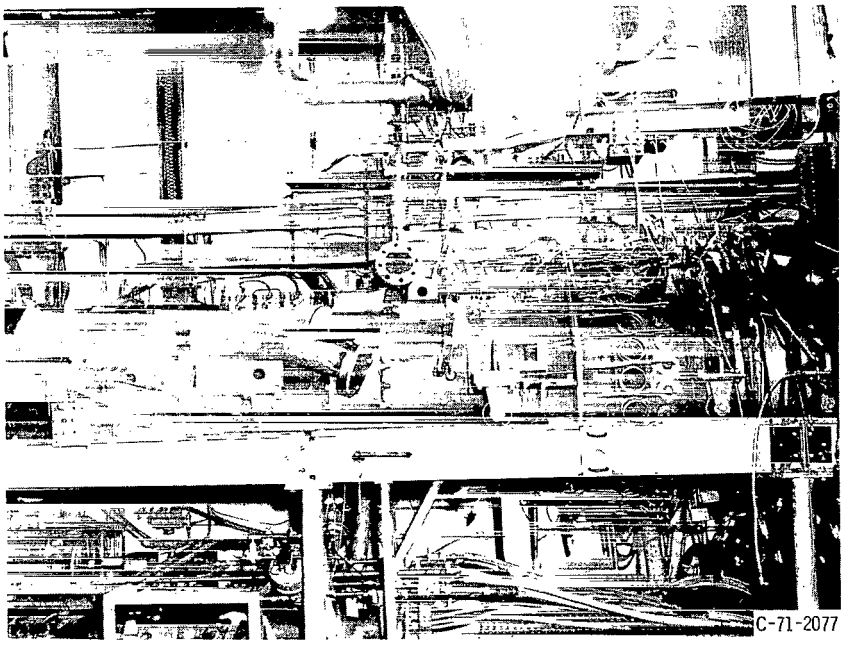

(b) Test section.

Figure 17. - Test section for advanced annular combustor.

APPENDIX D

INSTRUMENTATION

Measurement Methods

Measurements to determine combustor operation and performance were recorded by the Lewis Central Automatic Data Processing System (ref. 6). Control Room readout instrumentation (indicating and recording) was used to set and monitor the test conditions and the operation of the combustor. Pressures were measured and recorded by the central Digital Automatic Multiple Pressure Recorder (DAMPR) and by strain-gage pressure transducers (ref. 7). Iron-constantan thermocouples were used to measure temperatures between 240 to 675 K (-28° to 755° F), Chromel-Alumel thermocouples measured temperatures between 240 and 1560 K (-28° and 2350° F). High temperatures, 275 to 1920 K (35° to 3000° F) were measured with platinum-plus-13 percent-rhodium/platinum thermocouples. The indicated readings of all thermocouples were taken as true values of the total temperatures. The platinum-plus-13 percent-rhodium/platinum thermocouples were of the high-recovery aspirating type (ref. 8, type 6).

Airflow rates were measured by square-edged orifices installed according to ASME specifications. Fuel flow rates were measured by turbine flowmeters using frequency-to-voltage converters for readout and recording.

Instrumentation Stations

The locations of the combustor instrumentation stations are shown in figure 1. Instrumentation at inlet stations 3 and 3.5 is shown in figure 1(b). Inlet air temperature was measured by eight Chromel-Alumel thermocouples that were equally spaced around the inlet at station 3. Inlet air total pressure was measured by eight five-point total pressure rakes equally spaced around the inlet at station 3 and four five-point Pitot static tube rakes at station 3.5. The pressure rakes measured the total pressure profile at centers of equal areas across the inlet annulus. Static pressure at the inlet was measured by sixteen wall static pressure taps with eight on the outer and eight on the inner walls of the annulus at station 3 and the twenty statics associated with the Pitot tubes at station 3.5.

Combustor shroud instrumentation consisted of six rakes to measure airflow distribution between the outer, inner, and center flow passages as defined in figure 5. Each rake consisted of three total pressure tubes and a static pressure tube. These

rakes were located at the entrance to each flow passage and the tubes were at centers of equal area.

Combustor outlet total temperature and pressure at instrumentation station 4 were measured at 3^{o} increments around the exit circumference. At each 3^{o} increment, five temperature and pressure points were measured across the annulus. The water-cooled probe assembly containing the five temperature and pressure sensors is shown in figure 18. Three of these probes, each on an arm 120^{o} apart, rotated 120^{o} providing full coverage of the circumference. Water-cooled shields protected these probes when they were not in use at three fixed points in the exhaust stream. At these points, temperature and pressure were not measured. The probes were made of platinum-rhodium alloy where exposed to the hot exhaust gases. Also located at station 4 were eight wall static pressure taps.

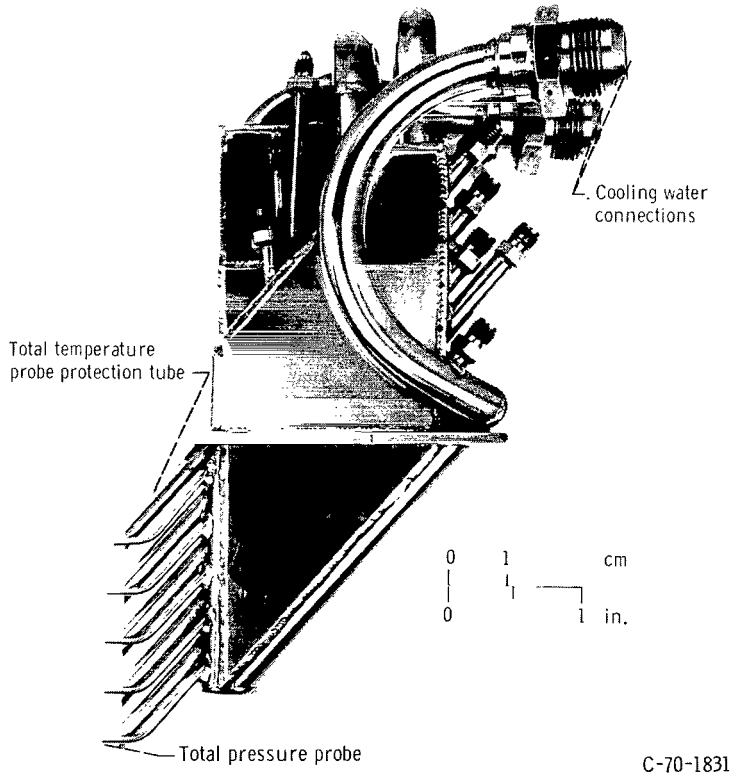

Figure 18. - Five-point total temperature and total pressure water-cooled probe assembly.

APPENDIX E

CALCULATIONS

Combustion Efficiency

Efficiency was determined by dividing the measure temperature rise across the combustor by the theoretical temperature rise. The theoretical rise is calculated from the fuel-air ratio, fuel properties, inlet air temperature, and pressure, as well as the amount of water vapor present in the inlet airflow. The exit temperatures were measured with five-point traversing aspirated thermocouple probes and were mass-weighted for the efficiency calculation. The indicated readings of all thermocouples were taken as true values of the total temperatures. The mass-weighting procedure is given in reference 5. In each mass-weighted average, 585 individual exit temperatures were used.

Reference Velocity and Diffuser Inlet Mach Number

Reference velocity V_{ref} for the combustor was computed from the total airflow, the maximum cross-sectional area between the inner and outer shrouds (see table IV), and the diffuser inlet using total pressure and temperature. Diffuser inlet Mach number was calculated from the total airflow; the total temperature, and the static pressure measured at the diffuser inlet, and the inlet annulus area.

Total Pressure Loss

The total pressure loss $\Delta P/P_{t3}$ was calculated by mass-averaging total pressures measured upstream of the diffuser inlet and at the combustor exit. The total pressure loss, therefore, includes the diffuser loss.

Exit Temperature Profile Parameters

Three parameters of interest in evaluating the quality of exit temperature profile are considered. Figure 19 is a graphical explanation of these parameters.

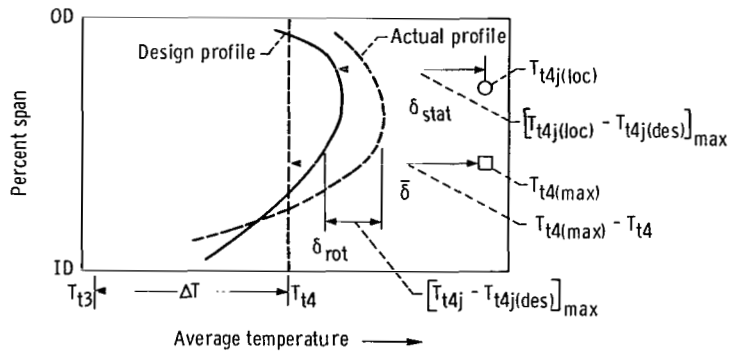

Figure 19. - Explanation of terms in exit temperature profile parameters.

The exit temperature pattern factor $\bar{\delta}$ is one parameter which is defined as

$$\bar{\delta} = \frac{T_{t4(max)} - T_{t4}}{T_{t4} - T_{t3}}$$

where T_{t4} and T_{t3} are averages of temperatures measured at the exit and inlet, and where $T_{t4(max)} - T_{t4}$ is the maximum temperature occurring anywhere in the combustor exit plane minus the average exit temperature. The parameter is useful for preliminary screening, but it does not take into account the desired radial temperature profile for which the combustor was designed. The desired average radial distribution of temperature at the combustor exit plane is determined by the stress and cooling characteristics of the turbine. For purposes of evaluating the double-annular combustor, an exit radial temperature profile was selected for conditions that are typical of advanced engines.

The two other parameters take the design profile into account. These parameters are

$$\delta_{stat} = \frac{\left[T_{t4j(loc)} - T_{t4j(des)}\right]_{max}}{T_{t4} - T_{t3}}$$

$$\delta_{rot} = \frac{\left[T_{t4j} - T_{t4j(des)}\right]_{max}}{T_{t4} - T_{t3}}$$

where $\left[T_{t4j(loc)} - T_{t4j(des)}\right]_{max}$ for δ_{stat} is the maximum positive temperature difference between the highest local temperature at any given radius and the design tempera-

ture for that same radius (subscript j refers to any radial location in the radial temperature profile) and where $\left[T_{t4j} - T_{t4j(des)}\right]_{max}$ for δ_{rot} is the maximum temperature difference between the average temperature at any given radius around the circumference and the design temperature for that same radius (see fig. 19). The term $T_{t4} - T_{t3}$ used in all three parameters is the average temperature rise across the combustor ΔT.

The parameter δ_{stat} is a measure of the quality of the exit temperature profile on the turbine stator, and δ_{rot} is a measure of the quality of the exit temperature profile on the turbine rotor.

Figure 20 is a model of a circumferentially distorted inlet air velocity profile. It is

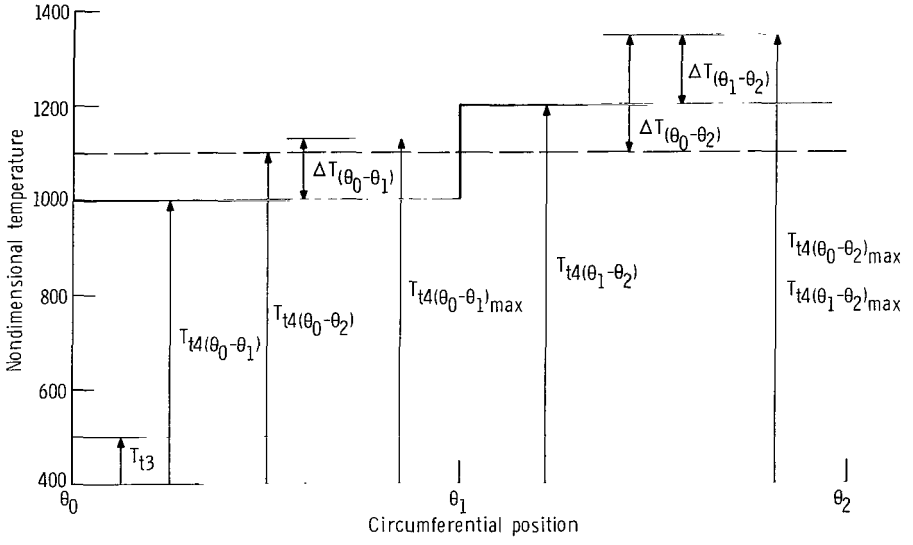

Figure 20. - Illustration of how a circumferentially distorted inlet air velocity profile increases pattern factor compared to radially distorted profiles where $\theta_0 \rightarrow \theta_1$ represents flat inlet velocity profile region and $\theta_1 \rightarrow \theta_2$ represents center peaked inlet velocity profile region.

drawn to illustrate the effect on pattern factor caused by circumferential inlet air velocity distortions compared to radial inlet air velocity distortions. On this figure additional subscripts will be found to correlate the exit temperature profile parameter of figure 19 to the special case presented in figure 20. The region of the curve from $\theta_0 - \theta_1$ (represented by subscripts $\theta_0 - \theta_1$) would correspond to a flat or moderately distorted inlet air velocity profile. Likewise the region of the curve from $\theta_1 - \theta_2$ (represented by subscripts $\theta_1 - \theta_2$) would correspond to a severe distortion. Note in the following calculation that the terms $\Delta T_{(\theta_0 - \theta_1)}$ and $\Delta T_{(\theta_1 - \theta_2)}$ in the figure have been selected to give equal pattern factors for the two regions, thus neither region's temperature profile

has been compromised. Figure 8(a) indicates that, on insensitive combustors such as this one, pattern factors are affected little by radial inlet air velocity profile.

The following computations show three methods of calculating the pattern factor for a circumferentially distorted inlet velocity profile which are: the normal way, calculating the pattern factor only in the $\theta_0 - \theta_1$ region, and calculating the pattern factor only in the $\theta_1 - \theta_2$ region. These calculations show a hypothetical increase in pattern factor of two-thirds from 0.25 to 0.417 resulting from simply combining two otherwise low pattern factor radial inlet air velocity profiles into one circumferentially distorted inlet air velocity profile. The equation for pattern factor is

$$\overline{\delta} = \frac{T_{t4(max)} - T_{t4}}{T_{t4} - T_{t3}}$$

and the normal computation of pattern factor is

$$T_{t4(max)} = T_{t4(\theta_0 - \theta_2)_{max}}$$

$$T_{t4} = T_{t4(\theta_0 - \theta_2)}$$

$$T_{t3} = T_{t3}$$

Thus,

$$\overline{\delta} = \frac{T_{t4(\theta_0 - \theta_2)_{max}} - T_{t4(\theta_0 - \theta_2)}}{T_{t4(\theta_0 - \theta_2)} - T_{t3}}$$

$$= \frac{1350 - 1100}{1100 - 500} \quad \text{(Numbers refer to fig. 20)}$$

$$= 0.417$$

Calculating the pattern factor only in $\theta_0 - \theta_1$ region is

$$T_{t4(max)} = T_{t4(\theta_0 - \theta_1)_{max}}$$

$$T_{t4} = T_{t4(\theta_0 - \theta_1)}$$

$$T_{t3} = T_{t3}$$

Thus,

$$\overline{\delta}_{(\theta_0 - \theta_1)} = \frac{T_{t4(\theta_0 - \theta_1)_{max}} - T_{t4(\theta_0 - \theta_1)}}{T_{t4(\theta_0 - \theta_1)} - T_{t3}}$$

$$= \frac{1125 - 1000}{1000 - 500}$$

$$= 0.25$$

and calculating the pattern factor only in $\theta_1 - \theta_2$ region is

$$T_{t4(max)} = T_{t4(\theta_1 - \theta_2)_{max}}$$

$$T_{t4} = T_{t4(\theta_1 - \theta_2)}$$

$$T_{t3} = T_{t3}$$

Thus,

$$\overline{\delta}_{(\theta_1 - \theta_2)} = \frac{T_{t4(\theta_1 - \theta_2)_{max}} - T_{t4(\theta_1 - \theta_2)}}{T_{t4(\theta_1 - \theta_2)} - T_{t3}}$$

$$= \frac{1350 - 1200}{1100 - 500}$$

$$= 0.25$$

Diffuser Inlet Velocity Profile

The diffuser inlet velocity profile was determined by calculating the velocity at each of the twenty total pressure tubes at station 3.5. Total temperature, static pressure, and total pressure measurements at that station were used for the calculation. To determine the $V_{3.5j}$ term, the four velocities at each radius were averaged. In like manner, the $V_{3.5}$ term is the average of the five $V_{3.5j}$ terms or the average of the twenty $V_{3.5j(loc)}$ positions. In the case of circumferential velocity profile plots, the $V_{(3 \text{ or } 3.5)j(loc)}$ term is velocity calculated at each total pressure tube position. In this case, the $V_{(3 \text{ or } 3.5)j}$ term is the average velocity at a given radius rather than the average of all total pressure measurements. It is assumed that the inlet total temperature is the same at both stations 3 and 3.5. The circumferential profile plots include data from both stations to present a more complete description of the profile. In this case, the total pressure is assumed to be nearly equal at both stations 3 and 3.5. The data at station 3 was obtained with forty total pressure tubes and sixteen wall static tubes.

Shroud Flows

For the shroud flows, an airflow was calculated for each total pressure tube all of which were located at centers of equal areas. The three airflows for each rake were summed. The two rakes in each annular passage were then averaged. The total shroud flow was determined by summing the average flow entering each passage. This flow was used to determine the percentage split between the three annular passages.

Units

The customary English system of units was used for primary measurements and calculations. Conversion to SI units (Systême International d'Unités) is done for reporting purposes only. In making the conversion, consideration is given to implied accuracy and may result in rounding off the values expressed in SI units.

REFERENCES

1. Perkins, J. Porter; Schultz, Donald F.; and Wear, Jerrold D.: Full-Scale Tests of a Short-Length, Double-Annular Ram-Induction Turbojet Combustor for Supersonic Flight. NASA TN D-6254, 1971.

2. Robbins, William H.; and Glaser, Frederick: Experimental Investigation of the Effect of Circumferential Inlet Flow Distortion on the Performance of a Five-Stage Axial-Flow Research Compressor with Transonic Rotors in All Stages. NACA RM E57J17, 1958.

3. Wear, Jerrold D.; Perkins, Porter J.; and Schultz, Donald F.: Tests of a Full-Scale Annular Ram-Induction Combustor for a Mach 3 Cruise Turbojet Engine. NASA TN D-6041, 1970.

4. Chamberlain, John: The Ram Induction Combustor Concept. Presented at the AIAA Third Propulsion Joint Specialist Conference, Washington, D.C., July 7, 1967.

5. Rusnak, J. P.; and Shadowen, J. H.: Development of an Advanced Annular Combustor. Rep. PWA-FR-2832, Pratt & Whitney Aircraft (NASA CR-72453), May 30, 1969.

6. Staff of the Lewis Laboratory: Central Automatic Data Processing System. NACA TN 4212, 1958.

7. Mealey, Charles; and Kee, Leslie: A Computer-Controlled Central Digital Data Acquisition System. NASA TN D-3904, 1967.

8. Glawe, George E.; Simmons, Frederick S.; and Stickney, Truman M.: Radiation and Recovery Corrections and Time Constants of Several Chromel-Alumel Thermocouple Probes in High-Temperature, High-Velocity Gas Streams. NACA TN 3766, 1956.

NASA-Langley, 1972 —— 28 E-6464

"The aeronautical and space activities of the United States shall be conducted so as to contribute . . . to the expansion of human knowledge of phenomena in the atmosphere and space. The Administration shall provide for the widest practicable and appropriate dissemination of information concerning its activities and the results thereof."

—NATIONAL AERONAUTICS AND SPACE ACT OF 1958

NASA SCIENTIFIC AND TECHNICAL PUBLICATIONS

TECHNICAL REPORTS: Scientific and technical information considered important, complete, and a lasting contribution to existing knowledge.

TECHNICAL NOTES: Information less broad in scope but nevertheless of importance as a contribution to existing knowledge.

TECHNICAL MEMORANDUMS: Information receiving limited distribution because of preliminary data, security classification, or other reasons.

CONTRACTOR REPORTS: Scientific and technical information generated under a NASA contract or grant and considered an important contribution to existing knowledge.

TECHNICAL TRANSLATIONS: Information published in a foreign language considered to merit NASA distribution in English.

SPECIAL PUBLICATIONS: Information derived from or of value to NASA activities. Publications include conference proceedings, monographs, data compilations, handbooks, sourcebooks, and special bibliographies.

TECHNOLOGY UTILIZATION PUBLICATIONS: Information on technology used by NASA that may be of particular interest in commercial and other non-aerospace applications. Publications include Tech Briefs, Technology Utilization Reports and Technology Surveys.

Details on the availability of these publications may be obtained from:

SCIENTIFIC AND TECHNICAL INFORMATION OFFICE

NATIONAL AERONAUTICS AND SPACE ADMINISTRATION

Washington, D.C. 20546